The immediate early protein 1 of the human herpesvirus 6B counteracts NBS1 and prevents homologous recombination repair pathways

Vanessa Collin[1,2,*], Élise Biquand[3,4,5,6,*], Vincent Tremblay[3,4,5], Élise Gaudreau-Lavoie[3,5], Julien Dessapt[3,4,5], Annie Gravel[1,2], Louis Flamand[1,2,†], Amélie Fradet-Turcotte[3,4,5,†]

[1] Division of Infectious Disease and Immunity, Centre Hospitalier Universitaire (CHU) de Québec-Université Laval Research Center, Quebec City, Quebec Canada, G1V 4G2;

[2] Department of microbiology, infectious disease and immunology, Faculty of Medicine, Université Laval, Quebec City, Quebec, Canada, G1V 0A6;

[3] Oncology Division, Centre Hospitalier Universitaire (CHU) de Québec-Université Laval Research Center, Quebec City, Quebec Canada, G1V 4G2;

[4] Department of molecular biology, medical biochemistry and pathology, Faculty of Medicine, Université Laval, Québec City, Quebec, Canada, G1V 0A6;

[5] Université Laval Cancer Research Center, Université Laval, Quebec City, Quebec, Canada, G1V 0A6;

[6] Current location: INSERM, Centre d'Étude des Pathologies Respiratoires (CEPR), UMR 1100, Tours, France – Université de Tours, Tours, France.

[*]Both authors contributed equally to this work

[†]Co-Corresponding authors:

E-mail: amelie.fradet-turcotte@crchudequebec.ulaval.ca

louis.flamand@crchudequebec.ulaval.ca

Keywords: DNA double-strand break signaling, telomere; integration; human herpesvirus 6A/B; immediate-early protein IE1.

Abstract

Integration of viral DNA in the genome of host cells triggers host-pathogens interaction that are consequential for the virus and the infected cells. In cells semi-permissive for viral replication, the human herpesvirus 6B (HHV-6B) integrates its genome into the host telomeric sequences. Interestingly, HHV-6B integration in gametes leads to a condition called inherited chromosomally integrated HHV-6B (iciHHV-6B), where the newborn carries a copy of HHV-6B in every cell of its body and is associated with health issues such as spontaneous abortion rates, pre-eclampsia and angina pectoris when transmitted to its offspring. Unlike retroviruses, the mechanism that leads to viral integration of DNA viruses and the consequences of these events on host cells are not well characterized. Here, we report that HHV-6B infection induce genomic instability by suppressing the ability of the host cell to sense DNA double-strand break (DSB). We discovered that this phenotype is mediated by the ability of the immediate-early HHV-6B protein IE1 to bind, delocalize, and inhibit the functions of the DNA damage sensor NBS1. These results raise the possibility that the genomic instability induced by the expression of IE1 from integrated genomes contributes to the development of iciHHV-6B-associated disease. As reported for other types of viruses, the inhibition of DSB sensing and signaling promotes viral replication. However, HHV-6B integration is not affected when this pathway is inhibited, supporting models where integration of the viral genome at telomeric sequence is dictated by mechanisms that promote telomere-elongation in a given infected cell and not solely DNA repair mechanisms.

Introduction

Human herpesvirus 6B (HHV-6B) is a betaherpesvirus that infects nearly 90% of the world's population in the first two years of life and is responsible for Roseola Infantum, a pathology defined by skin rashes, high fevers and respiratory distress(1–3). In this DNA virus subfamily, HHV-6B shares 94% homology with HHV-6A, another lymphotropic virus. Like other herpesviruses, HHV-6A and HHV-6B (HHV-6A/B) establish lifelong latency in infected hosts and can reactivate occasionally(4). However, whereas most herpesviruses achieve latency through the circularization and silencing of their genome, HHV-6A/B viruses can integrate their genome in the host chromosome terminal repeats called telomeres (chromosomally integrated HHV-6B (ciHHV-6B))(5, 6). If HHV-6A/B integration occurred in gametes before fertilization, the newborn carries a copy of HHV-6A/B in every cell of its body and can transmit it to its offspring. This condition called inherited chromosomally integrated HHV-6A/B (iciHHV-6A/B) concerns ~1% of the world's population, representing almost 80 million people(7, 8). iciHHV-6A/B is more prevalent in individual suffering from health issues such as spontaneous abortion rates(9), pre-eclampsia(10) and angina pectoris(11) compared to healthy subjects (reviewed in(12, 13)). However, consequences of iciHHV-6A/B are still poorly understood due to lack of clinical associations.

The linear double-strand DNA (dsDNA) genome of HHV-6A/B is flanked by an array of direct repeats containing 15 to 180 reiterations of 5'-TTAGGG-3' perfect telomeric repeats (pTMRs) that are identical to human telomeric sequences, and which are important for viral integration(14). HHV-6A/B genome integration occurs at telomeres in a process that is dependent on the integrity of these pTMRs(14). Based on this observation, current models propose that viral integration is mediated through homology-directed repair (HDR) processes including single stranded annealing (SSA) or break-induced replication (BIR)(15). These HDR pathways are favored given that the integration occurs in an oriented manner that is driven by one of the pTMR(14, 16). In this case, HHV-6A/B genome would integrate at sites of DNA double-stranded break (DSB) that are caused following replication fork collapse at telomeres upon replication stress. In both scenarios, the annealing of the pTMR sequence to the 3' overhang generated by partial resection of DNA ends of the telomere would drive integration(15, 17).

In mammalian cells, HDR uses homologous sequences as template to repair breaks in a faithful manner. During this process, broken DNA ends are first detected by the MRN complex (MRE11, RAD50, NBS1)(18). The accumulation of the MRN complex at the break induces a signaling cascade that leads to the activation of the serine–threonine kinase ataxia–telangiectasia mutated (ATM) and concomitant phosphorylation of the histone variant H2AX on Ser139 (γ-H2AX). The interaction of MDC1 with γ-H2AX then triggers the ubiquitylation of the chromatin that surrounds the break by promoting the accumulation of the E3- ubiquitin ligases RNF8 and RNF168(19, 20). In S/G2 phase of the cell cycle, the recruitment of the DNA repair factor BRCA1 and the nuclease CtIP to ubiquitylated chromatin cooperates with EXO1 and BLM-DNA2 nucleases to facilitate extensive end resection. Extensive accumulation of single-strand DNA (ssDNA) is generated through this process or by uncoordinated DNA unwinding, and DNA synthesis that occurs at stalled replication forks ultimately leading to the recruitment of recombinases that drive homology search(21). RAD51 or RAD52 recombinases promote DNA repair by HDR and SSA(22). Both recombinases also promote DNA repair of one-end DSB, but their exact contribution to that latter pathway is still unclear(23).

88 HHV-6A and B are two distinct viruses that share 90% sequence homology. Although they both have a
89 tropism for $CD4^+$ T lymphocytes, they present epidemiological, biological, and immunological differences(17).
90 HHV-6B, which infects nearly 90% of the population in the first two years of life, is much more characterized
91 than HHV-6A. HHV-6B expresses sequentially more than 97 proteins during its lytic cycle. Immediate early (IE)
92 proteins are expressed early in the viral cycle and exhibit functions that regulate viral genes expression and
93 promote the establishment of a favorable environment for infection. Interestingly, immediate early protein 1 (IE1)
94 transcripts are detected in RNA-seq analysis on tissues extracted from iciHHV-6B+ individuals(24), suggesting
95 that IE1 is expressed during latency. IE1 is the first protein expressed following HHV-6B infection(25) and
96 although it is known to control the antiviral immune response by compromising type I interferon production and
97 signaling(26, 27), its role during infection and the integration of the viral genome is still poorly defined. In infected
98 cells, IE1 is exclusively localized within promyelocytic leukemia (PML) nuclear bodies (PML-NBs) (28), a nuclear
99 structure that was recently implicated in DNA repair mediated by HDR through a yet undefined mechanism(29–
100 32). Interestingly, depletion of PML reduces HHV-6B integration(33), suggesting that the IE1/PML-NBs may
101 participate to viral integration.

102 In this study, we found that viral infection, and more specifically the expression of IE1, leads to the
103 accumulation of micronuclei and numerous DSBs in cells. Further investigations revealed that the viral protein
104 specifically prevents H2AX phosphorylation through a bipartite mechanism that relies on the ability of IE1 to
105 interact with NBS1 and inhibit its interaction with ATM. While this function is independent of PML, structure
106 function analysis identified a NBS1-interacting domain (NID) as well as NBS1-inhibitory domain (NBS1i) in the
107 N-terminus and the C-terminus regions of IE1, respectively. Although current models propose that viral
108 integration occurs through HDR DNA repair, we show that the expression of IE1 strongly inhibits all types of
109 repairs that rely on homology. We show that both viral replication and integration are not affected by the
110 depletion of NBS1 in cells where telomeres are elongated in a human telomerase reverse transcriptase (hTERT)
111 dependent manner, a finding that is consistent with a role of the telomerase complex in this process(34). In
112 contrast, in cells that rely on alternative telomere lengthening (ALT) mechanisms involving HDR events,
113 knockdown of NBS1 negatively affected HHV-6B integration. Thus, in addition to identifying a new bipartite
114 mechanism for the inhibition of NBS1 by a viral protein, our findings reveal that viral integration relies on
115 biological pathways that safeguard telomere extension in infected cells. Importantly, as IE1 expression has been
116 detected in cells where HHV-6A/B is integrated(35), our results suggest a potential role of genomic instability in
117 the development of diseases associated with iciHHV-6A/B.

118

119 **Results**

120 **HHV-6B infection and IE1 expression induce genomic instability**

121 Infection of the lymphoblast T cell line MOLT-3 (permissive for viral replication) by HHV-6B rapidly
122 induces the formation of micronuclei (MNi), suggesting that the virus leads to genomic instability during infection
123 (Fig.1*A* and *SI Appendix*, Fig.S1*A*). Among the early HHV-6B proteins that are expressed upon infection,
124 expression of IE1 in U2OS cell line is sufficient to promote the accumulation of MNi over time (Fig. 1*B* and *SI*
125 *Appendix*, Fig.S1*B*-*C*). Such MNi are compartmentally separated from the primary nucleus that are surrounded

126 by an envelope (*SI Appendix*, Fig. S1*D-E*). They arise from unresolved genomic instability such as DSBs (i),
127 lagging chromosome (ii) or by the rupture of anaphase bridges (ABs) (iii) (Fig. 1*C*)(36). Further analysis of the
128 IE1-induced MNi revealed that a much lower proportion of these MNi exhibit centromere staining (Fig. 1*D* and
129 *SI Appendix*, Fig. S1*F*), suggesting that they are not induced by chromosome segregation defects. Although
130 IE1 colocalizes with telomeres(37), fluorescence *in situ* hybridization revealed that IE1-induced MNi accumulate
131 similar levels of telomeric DNA than the micronuclei observed in parental U2OS cell (Fig. 1*E* and *SI Appendix*,
132 Fig. S1*G*). Moreover, IE1 is only detected in approximately 5-10% of these micronuclei (*SI Appendix*, Fig. S1*H*),
133 suggesting that micronuclei are not arising from IE1-induced genomic instability at telomeres. Interestingly,
134 metaphase spread assays revealed that IE1-expressing cells exhibit higher frequency of DNA breaks (Fig. 1*F-*
135 *G*), supporting the hypothesis that the micronuclei accumulation results from the accumulation of DSBs.

136

137 **HHV-6B impairs DSB-signaling by interacting with NBS1**

138 Accumulation of DSBs is either caused by increased source of DNA breaks or by defective DNA DSB-
139 signaling and repair. To determine how IE1 promotes genomic instability, we first investigated whether U2OS
140 clones that stably express the viral protein accumulate the DSB γ-H2AX marker. Surprisingly, γ-H2AX is
141 dramatically reduced following exposure to irradiation (IR) in cells that express IE1 (Fig. 2*A-B*). This inhibition
142 is independent of the accumulation of IE1 within PML-NBs as a similar phenotype is observed in PML-deficient
143 U2OS that transiently express IE1 ($PML^{-/-}$, Fig. 2*C* and *SI Appendix*, Fig. S2*A-C*). Importantly, the inhibition of
144 by IE1 is recapitulated in irradiated HHV-6B-infected MOLT-3 cells (Fig.2 *D-E*), indicating that DSB-signaling is
145 also impaired by IE1 in the context of a natural infection.

146 The histone variant H2AX is phosphorylated at DSBs following the activation of ATM by the MRN
147 complex(18). To determine how IE1 interferes with DSB-signaling, we first investigated the localization of NBS1
148 and MRE11 in U2OS clones expressing IE1. In the absence of irradiation, both NBS1 and MRE11 proteins
149 colocalize with IE1 foci (Fig. 3*A-D* and *SI Appendix*, Fig. S3*A*). Interestingly, only NBS1 is relocated to IE1 foci
150 following irradiation suggesting that the recruitment of MRE11 in absence of irradiation is mediated by NBS1
151 (*SI Appendix*, Fig. S3*B-C*). Consistent with this model, the recruitment of MRE11 to IEI foci is impaired in NBS1-
152 depleted U2OS cells that transiently express IE1 (*SI Appendix*, Fig. S3*D-F*). Furthermore, when mCherry-
153 LacRnls-IE1 fusion protein is recruited to a *LacO* array in U2OS 2-6-5 transfected cells(38, 39), only NBS1 is
154 recruited to the array with an efficiency similar to its recruitment to DSBs induced by the ER-mCherry-LacR-
155 FOKI-DD endonuclease, which is used as a positive control in this assay (Fig. 3*E-F* and *SI Appendix*, Fig. S3*G-*
156 *H*). The absence of γ-H2AX signaling at the array upon the recruitment of mCherry-LacRnls-IE1 shows that the
157 viral protein recruits NBS1 independently of DSB signaling. As observed in Fig. 2, the interaction of IE1 with
158 NBS1 is independent of its localization to PML-NBs as NBS1 is recruited to IE1 foci with a similar efficiency in
159 $PML^{-/-}$ U2OS cells (*SI Appendix*, Fig. S3*I-J*). Altogether, these results suggest that IE1 recruits NBS1 and inhibits
160 γ-H2AX signaling by preventing its recruitment to endogenous DNA breaks.

161

162 **Identification of NBS1 bipartite interaction and inhibition domain in IE1**

163 The functional domains of IE1 are not well characterized aside from a STAT2 binding domain that was
164 mapped in the N-terminal domain of the protein (amino acids 270-540)(26). Guided by a secondary structure
165 analysis of the protein, a series of IE1 fragments were fused to mCherry-LacRnls to assess their ability to recruit
166 endogenous NBS1 to the *LacO* array (Fig. 4*A*). Using this approach, we observed that the fragment comprising
167 amino acids (aa) 1-540 is sufficient to recapitulate the level of NBS1 recruitment observed with the full-length
168 protein (Fig. 4*B* and *SI Appendix*, Fig. S4*A*-*B*). In this assay, the C-terminal domain of the viral protein aa 541-
169 1078 was also able to partially recruit NBS1 to the *LacO*-array. As the fragment composed of aa 541-809 does
170 not promote NBS1 recruitment, we concluded that the domain 810-1078 also interacts with NBS1. Interestingly,
171 we found that only WT and the C-terminal (aa 541-1078) domain of IE1 were able to inhibit γ-H2AX signaling in
172 irradiated U2OS cells (Fig. 4*C*-*D* and *SI Appendix*, Fig. S4*C*). Together, these results suggest that IE1 interacts
173 and inhibits NBS1 using bipartite motifs. The N-terminal of IE1 is composed of a NBS1-interacting domain (NID)
174 and the C-terminal domain independently inhibits the ability of NBS1 to activate ATM (Fig. 4*A*). Based on this
175 observation, we named this C-terminal domain: NBS1 inhibitory domain (NBS1i).

176 NBS1 encodes a 95 kDa protein that contains multiple domains that are required for its recruitment to
177 DSBs and its interaction with the PI3K ATM and ATR(40). Briefly, NBS1 contains a forkhead-associated (FHA)
178 and two breast cancer C-terminal domains (BRCTs) that are both required for optimal phospho-dependent
179 accumulation of the protein at the break. The C-terminal part of the protein contains a domain that promotes its
180 interaction with MRE11 (MRE11-binding motif, MBM) and ATM (ATM-binding motif, ABM) (Fig. 4*F*). In the *LacO*-
181 LacR assay, the recruitment of mCherry-LacRnls NBS1 to the array is sufficient to promote the phosphorylation
182 of γ-H2AX(41), a function that is dependent of its ability to interact with ATM (Fig. 4*E*). Consistent with the
183 inhibitory function of IE1, expression of the viral protein is sufficient to inhibit NBS1-induced γ-H2AX signaling
184 at the array (Fig. 4*E* and *SI Appendix*, Fig. S4*F*). In this system, the mCherry-LacRnls-NBS1 328-754 was
185 unable to efficiently recruit IE1 to the array (Fig. 4*F*-*G* and *SI Appendix*, Fig. S4*G*), suggesting the IE1 interacts
186 with the BRCT2 domain of NBS1. Furthermore, LacR constructs that only lack the linker region also exhibits
187 reduced recruitment of IE1 to the array, suggesting that the interaction of IE1 with NBS1 also relies on the
188 integrity of this regions. Thus, our results support a model where IE1 need to contact two regions, the BRCA2
189 domain and the linker region. Whether both the NID and the NBS1i contact these regions or whether this is only
190 mediated by the NID is unknown.

191

192 **IE1 inhibits HDR repair pathways**

193 DSBs signaling is essential to trigger the activation of DNA repair pathways that have been proposed
194 to drive HHV-6B integration(15). As the functions of NBS1 are essential to promote the resection of DNA ends
195 that trigger homology-directed repair, we investigated whether IE1 interferes specifically with this process using
196 a panel of well-characterized DNA repair reporter assays. The efficiency of pathways that rely on homology-
197 based DNA repair was assessed using DR-GFP and CRISPR-LMNA assays (homologous recombination)(42,
198 43), a SA-GFP assay (single-strand annealing)(42) and a RAD51-dependent BIR-GFP assay (break-induced
199 replication)(44) (Fig. 5*A*-*C* and *SI Appendix*, Fig. S5*A*, top panels). In all assays, a condition without the
200 endonulease I-SceI was used as a negative control and the percentage of fluorescent-positive cells obtain with
201 I-SceI was set to 1. Consistent with the ability of IE1 to inhibit the function of NBS1, both transient and stable

202 expression of the viral protein drastically abolished all types of homology-directed DNA repair (Fig. 5*A-C*, lower
203 panel, and *SI Appendix*, Fig. S5*A-C*). As the clonal BIR-GFP U2OS cell line was generated in this study using
204 previously described BIR-GFP reporter plasmid(44), we used siRNAs against RAD51 and RAD52 as additional
205 controls (*SI Appendix*, Fig. S5*D-F*)(23). As expected, BIR-GFP signal was specifically inhibited in cells depleted
206 for RAD51(44). In contrast to homology-based DNA repair, IE1 only slightly decreased or increased DNA repair
207 in reporter assays that assess the efficiency of NHEJ (NHEJ-GFP EJ7 Fig. 5*D*, and NHEJ-pc222 *SI Appendix*,
208 Fig. S5*G*). Altogether, these results are consistent with a model where homology-based DNA repair is
209 specifically inhibited in cells that express HHV-6B IE1 and raise the point that either integration occurs in a
210 context when the expression of the viral protein is minimal, absent, or driven through a homology-independent
211 mechanism.

212

213 **Integration of HHV-6B relies on the pathway that safeguards telomere elongation**

214 The MRN complex is commonly targeted by viruses to promote viral replication(45) however, the
215 requirement of this complex for viral integration is unclear. HHV-6B infection leads to different outcomes
216 depending on the nature of the infected cells (Fig. 6*A*). In permissive cells, the expression of viral proteins
217 promotes viral replication (lytic state). In contrast, in semi-permissive cells, integration of the viral genome at
218 host's chromosome telomere is favored. The factors that lead to the reactivation of the integrated viral genome
219 are still misunderstood. The fact that HHV-6B IE1 evolved to inhibit the function of NBS1 raises the possibility
220 that the DNA repair protein negatively impact viral replication and/or integration. To investigate the role of NBS1
221 in these processes, permissive cells (MOLT-3) and semi-permissive cells (U2OS, HeLa, and GM847) depleted
222 or not for NBS1 were infected with HHV-6B (*SI Appendix*, Fig. S6*A-D*). In MOLT-3, increased replication is
223 measured in cells depleted for NBS1, suggesting that the protein is detrimental for HHV-6B replication (Fig. 6*B*).
224 Interestingly, our results suggest that viral integration in semi-permissive cells relies on the molecular
225 mechanisms that drive telomere elongation in these cells. Indeed, integration was not affected by the depletion
226 of NBS1 in cells where telomeres lengthening is secured by hTERT (Table 1). However, integration is
227 significantly reduced upon NBS1-depletion in both cell lines that rely on Alternative Lengthening of Telomeres
228 to maintain telomere length (Table 1). In ALT-positive (ALT+) cells, telomere maintenance occurs on break-
229 induced telomere synthesis, a RAD51-independent homology-directed DNA repair pathway(46). Thus, our data
230 support a model in which the mechanism of viral integration is dictated by the telomere lengthening pathway of
231 the infected semi-permissive cell rather than a common mechanism only driven by viral protein. Importantly, our
232 data also imply that the expression of IE1 must be repressed to promote integration in ALT+ cells.

233

234 **Table 1.** Importance of NBS1 for HHV-6B chromosomal integration in ALT + and – cells.

Cell lines	ALT status	shRNA	% of cells integrated HHV-6B[a] (n)[b]	P value[c]
HeLa	Negative	CTRL	0.96 (36320)	$<2.2e^{-16}$
		NBS1	6.11 (33280)	
GM847	Positive	CTRL	0.65 (21820)	$<2.2e^{-16}$
		NBS1	0.01 (18320)	
U2OS	Positive	CTRL	1.60 (20000)	$<2.2e^{-16}$

		NBS1	0.69 (21520)	
U2OS PML$^{-/-}$	Positive	CTRL	0.71 (28220)	ns
		NBS1	0.78 (30460)	

[a] mean of three independent cultures

[b] total number of cells analyzed

[c] Pearson's Chi-squared test with Yates' continuity correction

Discussion

In this study, we set out to understand two phenomena in HHV-6B; 1) the molecular mechanism by which HHV-6B induces genomic instability in infected cells, and 2) the role of HDR-mediated repair pathways in the establishment of the latent state in semi-permissive cells. Using a series of microscopy- and cytometry-based approaches to track the source of DNA breaks in infected cells and in cells expressing the immediate-early protein IE1, we discovered that in both conditions, DNA double-strand break signaling, and repair are strongly inhibited through interference with the recruitment of the DNA repair protein NBS1 at the breaks. Specifically, we defined the molecular mechanism by which IE1 triggers the redistribution of the MRN complex to IE1-PML NBs by using a single-cell assay in which the colocalization of DNA repair factors with mCherry-tagged viral proteins is restricted to an integrated *LacO* array. These findings revealed that IE1 specifically interacts with NBS1 through a NBS1-interacting domain (NID) that is located in the N-terminal part of the viral protein. Furthermore, our finding revealed that the activation of ATM by NBS1 is strongly inhibited by a NBS1-inhibitory domain (NBS1i) located in the C-terminal region of IE1, supporting a model where IE1 impairs the function of NBS1 through bipartite motifs. Consistently, we found that the expression of IE1 specifically abolishes NBS1-dependent DNA repair pathways by using an array of well-established DNA repair reporter assays. Altogether, our work argues against a model where viral integration is promoted solely by homology-based repair, but rather supports models where integration of the viral genome at telomeres is dictated by mechanisms that promote telomere-elongation in a given infected cell. Our work suggests that IE1 expression must be tightly regulated to enable viral integration in cells where telomeres are elongated by ALT. Finally, our results raise the possibility that expression of IE1 from integrated genomes might contribute to the development of iciHHV-6B associated disease by inducing genomic instability in these cells. Using an RNA-seq approach, Peddu et al. reported that the *IE1* gene is among the most abundantly expressed genes in a variety of tissues from iciHHV-6+ individuals(47). Spontaneous and inducible IE1 protein expression from integrated HHV-6 genomes was also documented(35). At present, diseases associated with iciHHV-6A/B status include increased spontaneous abortion rates(9), pre-eclampsia(10) and angina pectoris(11). Further characterization of the proteins expressed from integrated genomes as well as the disease associated with these conditions will be required to strengthen our understanding of the consequences associated with viral latency in iciHHV-6B subjects.

The functions of the MRN complex are required at DSBs, stalled replication forks, chromosome segregation and dysfunctional telomeres to safeguard genomic stability in cells(18, 48). Viruses have evolved different strategies to adapt to their host cell environment. Many of them developed specific mechanisms to manipulate DNA damage signaling to either promote viral processes such as replication and integration, or to protect the integrity of their genome upon infection(45). A classic example comes from adenoviruses, where the

272 MRN complex is targeted by multiple viral protein to inhibit its function. Specifically, E4-ORF3-dependent
273 relocalization of MRN proteins and E4-ORF6/E1B-55K-dependent degradation of MRN components is essential
274 to enable transduction and efficient viral replication(49–54). In contrast, other viruses such as adeno-associated
275 virus (AAV) rely on the activity of the complex for the integration of their genomes at the human AAVS1 site(55)
276 or to promote a DNA damage response that enhances infection levels (Herpes Simplex Virus 1 (HSV-1) and
277 Human Papillomavirus (HPV))(56–59). While these findings demonstrate that some viruses hijack the function
278 of DNA repair protein to support different steps of the infection, the mechanisms by which these processes
279 benefit viral replication remain a long-standing mystery in the field(45). In this study, we report that depletion of
280 NBS1 results in increased HHV-6B replication in permissive cells, suggesting that HHV-6B also evolved to
281 interfere with NBS1, or with the MRN complex, to prevent undesired recognition of viral DNA as broken DNA.
282 This makes sense considering that during viral replication, numerous double-stranded linear genomes, which
283 can be perceived as broken DNA, are generated. Interestingly, our structure function analyses revealed that the
284 interaction between IE1 and NBS1 is mainly driven by the BRCT2 domain (aa 201-326) of NBS1 and, to a lesser
285 extent, by the linker region (aa 327-638). These findings thus revealed that IE1 interacts with a domain of NBS1
286 that is essential for its MDC1-dependent chromatin retention of NBS1 to DSB (BRCT2)(60–64), providing a
287 rational for its ability to compete with the recruitment and function of the DNA sensor protein. Interestingly, it
288 has been proposed that the viral protein HSV-1 ICP0 also interacts with NBS1 through a region that span the
289 linker (aa 590-710) to redirect HDR to specific loci during the infection(65). Here, the ability of IE1 to actively
290 inhibit the NBS1-dependent activation of ATM at the *LacO* demonstrates that this is not the case for IE1 unless
291 the NBS1i domain is post-translationally regulated during the infection. In contrast to AAV integration at the
292 AAVS1 locus, the integration of HHV-6B at telomere is not strictly dependent on the MRN complex but rather
293 on processes used by infected cells to elongate telomeres (discussed below). Recent work by Tan et al.
294 revealed that activation of DNA damage response is required to trigger a robust type I interferons response
295 (IFNs) following mitochondrial DNA damage(66), it is thus highly plausible that viruses evolved to interfere with
296 the activation of the DDR in order to counteract the activation of an efficient antiviral response in infected cells.
297 This type of IFNs activation is different from the nuclear factor κβ (NF-κβ)-dependent IFNs production that rely
298 only on MRE11 and RAD50(18). Further studies will be required to investigate this possibility as well as the
299 requirement of NSB1 for this process.

300 In germline, hematopoietic, stem and rapidly renewing cells, telomere elongation relies on the hTERT,
301 a polymerase that catalyzes the extension of telomeric DNA repeats using RNA as template(67). While hTERT
302 is negatively regulated in somatic cells, senescence is overcome in cancer cells either through the re-activation
303 of the hTERT enzyme or by an alternative homology-directed mechanism called ALT(68). The HHV-6B genome
304 contains conserved telomeric sequences that are required for viral integration(14). In this study, we show that
305 HHV-6B integration is independent of NBS1 in ALT- cells while it is dependent on NBS1 in ALT+ cells. These
306 findings are consistent with previous report showing that the telomerase complex is required for optimal HHV-
307 6B integration(34) as well as with the role of NBS1 in ALT (69, 70). While PML is not required for the interaction
308 of IE1 with NBS1 and the ability of IE1 to inhibit the phosphorylation of H2AX (this study), NBS1 is required for
309 the assembly of functional ALT-associated PML bodies(71). These concomitants roles are in line with the
310 absence of phenotype associated with NBS1-depletion in integration assay performed on PML$^{-/-}$ ALT+ U2OS.
311 Intriguingly, we previously report that PML KO also reduces integration in the ALT- HeLa cells, reinforcing the

312 hypothesis that PML plays ALT-independent role in this process(33). Further studies will be required to elucidate
313 this function.

314 In line with previous findings showing that HHV-6B integration is not altered upon inhibition of
315 RAD51(72, 73), we found that IE1 inhibits homology-driven repair processes, and that integration is independent
316 of NBS1 in ALT- cell lines. Together, these observations argue against models where integration mechanisms
317 rely on RAD51-dependent BIR or SSA(74). However, it is important to note that all homology-directed reporter
318 assays used in this study rely on extensive DNA end resection following the induction of breakage by the
319 nucleases I-SceI or Cas9, a process that is dependent on NBS1(75). Thereby, integration models where SSA
320 or RAD51-independent BIR trigger integration following extensive accumulation of single-strand DNA generated
321 at stalled replication fork are still plausible. One attractive model is that the integration of HHV-6B occurs during
322 mitotic DNA synthesis (MiDAS), a RAD52-dependent BIR mechanism that is initiated upon replication fork stall
323 that remain unresolved at the start of mitosis, a problem often observed at DNA locus that are hard to replicate
324 such as telomeres(9, 23, 76). Such mechanism is NBS1- and RAD51-independent and is mediated by RAD52,
325 POLD3 as well as the structure-specific nuclease MUS81-EME1. Alternatively, upon entry into a cell and before
326 the viral genome circularizes (and before IE1 is expressed), the viral DNA can be perceived as broken DNA.
327 Under such circumstances, the MRN complex would be recruited to the ends of the viral genome and initiate
328 3'→ 5' resections. The ssDNA ends of eroded telomere (no longer efficiently protected by the shelterin complex)
329 could anneal to the near terminal telomeric sequence at the right end of the genome in a process analogous to
330 an ALT mechanism described in yeast (reviewed in (23)). Once the entire viral genome is copied, the telomeric
331 repeats at the left end of the genome would serve as template for telomerase or ALT mechanisms to regenerate
332 a telomere of appropriate length(77).

333 In conclusion, we provide a detailed characterization of the HHV-6B IE1 protein as an efficient inhibitor
334 of DSB-signaling through the recruitment of NBS1. As such, IE1 contributes to the favorable establishment of a
335 productive infection. Despite being a relatively abundant protein expressed very early upon entry, the functions
336 of IE1 remain poorly defined. IE1 shares very little sequence homology with proteins from other herpesviruses
337 (except HHV-6A and HHV-7) meaning that deductions based on primary sequence analysis are very limited.
338 Our work adds to the growing knowledge surrounding HHV-6B integration processes and the potential
339 importance of the IE1 protein during the infectious process.

340

341 **Material and Methods**

342 **Plasmids and virus**

343 pcDNA4/TO/myc-His-HHV-6B IE1 was previously described (27). The PiggyBac transposon-based (PB)-TetO
344 and the PB-CA-rtTA-IRES-NEO plasmids were generated as previously described(78). PB-TetO-HHV-6B IE1,
345 mCherry-LacR and GFP expression vectors were generated using Invitrogen™ Gateway™ recombination
346 cloning (Invitrogen) and the following destination vectors: pDEST-PB-TetO (78), pDEST-mCherry-LacR (79) or
347 pDEST-FRT-TO-GFP (80). HHV-6B IE1 was PCR amplified from pcDNA4/TO-HHV-6B IE1. HHV-6B IE1
348 fragments (aa1-1078, aa1-809, aa1-540, aa541-809, and aa541-1078) and NBS1 fragments (aa1-754, aa1-
349 733, aa1-638, aa1-327, aa109-754, aa201-754, and aa328-754) were PCR amplified from pcDNA4/TO-HHV-

350 6B IE1 and pLXIN2-NBS1, a kind gift from Cary A. Moody (University of North Carolina at Chapel Hill, North-
351 Carolina) (81). HHV-6B strain Z29 (82) was produced by our laboratory, as previously described(83). A list of
352 the plasmids that were used in this study is provided in Table S3.
353
354 **RNA interference**
355 SMARTPool siRNA targeting RAD51 and a non-targeting single siRNA duplex sequences were purchased from
356 Dharmacon. Single siRNA duplexes targeting RAD52 was a kind gift from Jean-Yves Masson (Université Laval,
357 Québec, Canada). siRNAs were transfected in a forward transfection mode 24 hours prior to cell processing
358 using RNAimax (Invitrogen) according to the manufacturer's protocol. Plasmids carrying a NBS1 short hairpin
359 RNA (shNBS1) (TRCN0000010393, Open Biosystems) or a control shRNA (shCTRL) (Mission® TRC2 pLKO.5-
360 puro non-mammalian shRNA control plasmid DNA, Sigma #SHC202) in the pLKO background backbone were
361 a kind gift from Cary A. Moody (University of North Carolina at Chapel Hill, North-Carolina) (81). Lentiviruses
362 were produced as previously described (81). Briefly, plasmids expressing shRNAs with vesicular stomatitis virus
363 G (pMD2.g) and lentiviral packaging (pPAX) plasmids were co-transfected into HEK-293T cells using
364 polyethyleneimine (PEI). 48-72 hours post-transfection, supernatants containing lentivirus were harvested and
365 U2OS, MOLT-3, HeLa, and GM847 were transduced in the presence of 8 µg/ml hexadimethrine bromide
366 (Polybrene) (Sigma). Knockdown of RAD51, RAD52 and NBS1 were confirmed for each experiment by Western
367 blotting or qPCR analyses.
368
369 **Cell Culture and transfections**
370 Cell lines were maintained at 37ºC and 5% CO_2. All culture media were supplemented with 10% fetal bovine
371 serum (FBS). MOLT-3 (American Type Culture Collection, ATCC) were cultured in Roswell Park Memorial
372 Institute (RPMI-1640; Corning Cellgro), 8.85 mM HEPES and 5 µg/ml plasmocin (Invivogen). GM847 and HeLa
373 cell lines were obtained from ATCC and cultured in Dulbecco's Modified Eagle's Medium (DMEM; Corning
374 Cellgro), NEM (Corning Cellgro), 8.85 mM HEPES, and 5 µg/ml plasmocin (Invivogen). U2OS (U2OS, obtained
375 from ATCC), U2OS PML$^{-/-}$ (37), U2OS 2-6-5 (Gift from Roger Greenberg, University of Pennsylvania,
376 Philadelphia)(39), U2OS DR-GFP, NHEJ-GFP (EJ7), and SA-GFP (Gift of Jeremy Stark (City of Hope National
377 Medical Center, California)(84, 85), and U2OS NHEJ-pc222 (Gift from Jacques Côté (Université Laval,
378 Québec)(86) cell lines were cultured in McCoy's medium (Life Technologies). Doxycyclin-inducible U2OS HHV-
379 6B IE1 clones 10 and 102 (C10 and C102) were established by co-transfecting PB-TetO-HHV-6B IE1, pCMV-
380 hypBAse and PB-CA-rtTA-IRES-NEO plasmids, at a DNA ratio of 1:1:1 in the U2OS SA-GFP cell line using
381 Lipofectamine 2000 (Invitrogen) according to the manufacturer's protocol. Clones were selected using 40
382 mg/mL of G418 and isolated using a limit dilution approach. U2OS BIR were established with a GFP-based
383 reporter plasmid (pBIR-GFP) containing already characterized I-Sce1 reporter cassette to monitor BIR(87).
384 Plasmid transfection was carried out using Lipofectamine 2000 (Invitrogen) according to the manufacturer's
385 protocol. Clones were selected using 2 µg/ml puromycin and isolated using a limit dilution approach.
386 Experiments were performed with a stable reporter clone which produce between 1.5% and 3% of GFP-positive
387 cells after DSBs induction. Unless indicated otherwise, expression of IE1 was induced by adding 1 µg/ml
388 doxycycline for 48h. HeLa DR-GFP (Gift from Roger Greenberg, University of Pennsylvania, Philadelphia) and
389 HEK293T cell lines were cultured in Dulbecco's modified Eagle's medium (DMEM) (Life Technologies). All cell

390 lines were validated using short tandem repeat (STR) markers and tested negative for mycoplasma
391 contamination.
392
393 **Chemicals and sources of DNA damage**
394 Doxycycline (Dox, 1 µg/ml, D3447, Sigma) was used to induce the production of HHV-6B IE1 in stable U2OS
395 cell lines C10 and C102 for 48h. In the FOK1 system, DSBs were created at the LacO array by promoting the
396 nuclear localization (4-Hydroxytamoxifen (4-OHT, 100 nM, #3412, Tocris)) and stabilization (Shield-1 ligand,
397 0.5 µM, CIP-S1-0001, CheminPharma)) of mCherry-LacR-FOK1 nuclease fused to a destabilization domain
398 (DD) and to a modified estradiol receptor (ER) (ER-mCherry-LacR-FOKI-DD) for six hours prior to
399 immunofluorescence sample preparation. DNA damage were induced by exposing cells to ionizing irradiation
400 (IR). U2OS were exposed to 1 Gy with a CellRad (Precision X-Ray Inc.) and MOLT-3 to 4 Gy with the
401 Gammacell® 40 Exactor (Best Theratronics Ltd.).
402
403 **Viral infection and integration assays**
404 For immunofluorescence assays on viral infection, 1 x 10^6 MOLT-3 cells were pelleted, infected or not (Mock)
405 at a multiplicity of infection (MOI) of 1 with HHV-6B (strain Z29) and resuspended at final concentration of 1 x
406 10^7 cells/ml with fresh RPMI in a 1.5 ml tube for 5 hours at 37°C, 5%. The MOLT-3/HHV-6B prep was mixed
407 every 30 minutes by flickering the tube. Cells were then washed three times in phosphate-buffered saline (PBS)
408 and resuspended in 1 ml of fresh RPMI in a 12-well plate. Twenty-four hours post-infection, cells were processed
409 for immunofluorescence. For viral replication, 1.5 x 10^6 of MOLT-3 cells were pelleted into a 1.5 ml tube and
410 infected or not (Mock) at a MOI of 1 with HHV-6B for 5 hours as described above. After 3 washes with PBS cells
411 were resuspended in 3 ml of fresh RPMI, in a 6-well plate. At the indicated time point, 0.5 x 10^6 cells were
412 harvested and processed for DNA extraction using QIAamp DNA Blood Mini Kit as described by the
413 manufacturer (Qiagen Inc.) and analysed by qPCR. Integration assays were performed as described
414 previously(88). Briefly, 1 x 10^4 cells/well (U2OS shCTRL, U2OS shNBS1, HeLa shCTRL, HeLa shNBS1, GM847
415 shCTRL, GM847 shNBS1), cells were infected at MOI of 1 with HHV-6B in a 24-wells plate for 24 hours and
416 washed with PBS 1X 3 times. Cells were then seeded in 6-well plates and passaged for 4 weeks prior to DNA
417 extraction with the QIAamp DNA Blood Mini Kit as described by the manufacturer (Qiagen Inc.) and analyzed
418 by ddPCR.
419
420 **Quantitative PCR (qPCR) and droplet digital PCR (ddPCR) analyses**
421 qPCR was performed as previously described (83). DNA was analyzed using primers and probes against *U67-*
422 *68* (HHV-6B) and *RPP30* (reference gene). Data were normalized against the corresponding genome copies of
423 the cellular *RPP30* gene. ddPCR was used to quantify integration frequency as previously described (88).
424 Briefly, the HHV-6B chromosomal integration frequencies were estimated assuming a single integrated HHV-
425 6/cell and calculated with the following formula: (number of HHV-6 copies)/(number of RPP30 copies/2 copies
426 per cell) × 100, as previously described. This assay was previously extensively validated and provide
427 comparable data to single cell cloning and quantification.
428
429 **RNA extraction and RT-qPCR**

430 Total RNAs were extracted with the RNeasy mini kit following manufacturer's instructions (QIAGEN) and
431 quantified by nanoDrop. 250-500 ng of total RNA was reverse transcribed with the High-Capacity cDNA reverse
432 transcription kit (Invitrogen) according to the manufacturer's instructions. Contaminant genomic DNA was
433 removed by DNaseI (ThermoFisher) incubation prior to the reverse transcription (RT) reaction and confirmed
434 by GAPDH RT-PCR performed on DNaseI treated reactions. qPCR was performed using the LightCycler 480
435 apparatus (Roche) with the LightCycler 480 SYBR Green 1 qPCR master mix (Roche) using the following
436 program: 40 cycles of 94 °C denaturation for 15 sec, 56 °C annealing for 5 sec and 72 °C elongation for 15 sec.
437 5% of the RT-PCR reaction was used as template. Standard curve was performed with serial dilution using the
438 U2OS cDNA as template. Relative expression of each gene was determined using the standard curve and
439 normalized to the relative expression of the GADPH. The primers are listed in Table S1.
440
441 **Immunofluorescence microscopy**
442 One hour post-irradiation, MOLT-3 cells were pelleted, washed 3 times in PBS and 1 x 10^4 cells were added to
443 each well of a microscope slide with 10 reaction wells (MP Biomedicals™ Multitest Slides, Fisher Scientific #
444 ICN6041805). Once dried, cells were fixed for 20 minutes at room temperature with 2% paraformaldehyde
445 (PFA), hydrated for 5 minutes with PSB and processed for immunofluorescence. U2OS and U2OS 2-6-5 cells
446 were grown in 24-well plates on glass coverslips and fixed 24 hours later with either 2% (wt/vol) PFA in PBS for
447 20 minutes at room temperature or with 100% MeOH for 20 minutes at -20°C. When indicated, cells were treated
448 with the indicated amount of Gy, 15 min or 1 hour prior to fixation. For immunostaining with anti-NBS1 and anti-
449 MRE11 antibodies, nuclear extraction with ice-cold NuEx buffer (20 mM HEPES pH 7.4, 20 mM NaCl, 5 mM
450 MgCl2, 0.5% NP-40, protease inhibitors (Complete, EDTA-free protease inhibitor, Sigma), and 1 mM DTT) for
451 20 min on ice for prior to fixation. U2OS PFA-fixed cells were further permeabilized with 0.3% (vol/vol) Triton X-
452 100 for 20 minutes at room temperature. MOLT-3 and U2OS fixed cells were incubated with blocking buffer (2%
453 BSA in PBS or 0.1% BSA, 3% goat serum, 0.1% Triton, 1 mM EDTA pH 8.0 in PBS) for 30 minutes at room
454 temperature and then incubated with primary antibodies (Table S2) diluted in blocking buffer for 2 hours at room
455 temperature, followed by washes in PBS. Next, cells were incubated for 1 hour at room temperature with
456 secondary antibodies diluted in blocking buffer and counterstained with 4',6-diamidino-2-phenylindole (DAPI,
457 0.4 µg/mL) in PBS. Cells were washed with PBS 1X and the coverslips were mounted onto glass slides with
458 Prolong Diamond mounting agent (Invitrogen). To visualize micronuclei in MOLT-3 infected or control cells, cells
459 were collected processed with an hypotonic solution (75 mM KCl) for 20 minutes at 37°C. Cell were then fixed
460 with fresh 3:1 methanol:acetic acid for 5 minutes and washed three time with 3:1 methanol:acetic acid solution.
461 Washed pellets were resuspended in 500µl of 3:1 methanol:acetic acid, dropped on a microscope slide and air
462 dried prior to DNA counterstaining with DAPI. Images were either taken using a Zeiss LSM700 (and LSM900
463 recently acquired) laser-scanning microscope equipped with a 63x oil lens or a Wave FX-Borealis - Leica DMI
464 6000B microscope with the camera Image EM (Hamamatsu, 512x512 pixels) and Orca-R2 (Hamamatsu,
465 1344x1024 pixels) with a 40x (Quorum Technologies). Images were analyzed and quantified using ImageJ
466 software [National Institutes of Health (NIH)]. In micrographs, dashed lines indicated nucleus outlines when
467 DAPI is not shown. Unless stated otherwise, insets represent 10 X magnifications of the indicated fields.
468
469 ***in situ* hybridization (FISH)**

470 Fixed cells were processed as described for immunofluorescence staining and then fixed for 2 minutes at room
471 temperature with 1% PFA/PBS. Coverslips were washed twice with PBS for 5 minutes and dehydrated for 5
472 minutes in successive ethanol baths (70%, 95%, 100%). Once dried, coverslips were placed upside down on a
473 drop of hybridizing solution (70% formamide; 0.5% blocking reagent; 10 mM Tris-HCl pH 7.2; 1/1000 Cy5-TelC
474 PNA probe (F1003, PNABio, Newbury Park, CA, USA)). Sample were denatured for 10 minutes at 80ºC on a
475 heated block. Coverslips were incubated over night at 4ºC and kept in the dark. After hybridization, coverslips
476 were washed two times for 15 minutes in washing solution (70% formamide; 10 mM Tris-HCl pH 7.2) and then
477 washed 3 times for 5 minutes with PBS. Sampled were air dried, counterstained with DAPI, washed with PBS
478 and coverslips were mounted onto glass slides with Prolong Gold mounting agent (Invitrogen).
479
480 **Metaphase spread analysis**
481 U2OS SA-GFP HHV-6B IE1 cells were arrested in mitosis using 1 µM nocodazole for 3 hours at 37°C and 5%
482 CO_2. Cells were then resuspended and incubated in pre-warmed hypotonic solution (KCl 75 mM, 15% SVF) at
483 37°C for 15 minutes to induce swelling and fixed in (75% ethanol, 25% acetic acid) overnight at 4ºC. Droplet of
484 cells were spread onto glass slides pre-cooled at -20ºC and dried overnight in the dark at room temperature.
485 Slide were then mounted with Vectashield Antifade Mounting Medium containing DAPI (VECTH20002, MJS
486 BioLynx Inc.). Images were taken using a Zeiss LSM700 laser-scanning microscope equipped with a 40x water
487 lens. Quantification was done on 3 biological replicates and 10 spreads were quantified per experiments.
488
489 **Reporter-based DNA repair assays**
490 For DR-, NHEJ-, SA-, and BIR-GFP reporter assays in which HHV-6B IE1 was transiently transfected, U2OS
491 or HeLa cells carrying the respective GFP expression cassette were plated at 125 000 cells/well in a 6 well
492 plates. Twenty-four hours later, cells were co-transfected with the indicated combination of plasmids:
493 pcDNA4/TO-HHV-6B IE1 along with I-SceI plasmid (pCBASceI, Addgene #26477). The pcDNA4/TO/myc-His
494 vector was used as negative control for conditions without I-SceI or IE1. A plasmid expressing iRFP was also
495 transfected to correct for transfection efficiency in each assay. For the NHEJ-GFP (EJ7) assay, cells were co-
496 transfected with Cas9 and sgRNA-expressing vectors p330X-sgRNA7a and p330X-sgRNA7b expressing
497 plasmids instead of I-SceI(85). After 48 hours (or 72 hours for NHEJ-GFP (EJ7)), cells were trypsinized,
498 harvested, washed and re-suspended in PBS. The percentage of GFP-positive in iRFP-positive cells was
499 determined by flow cytometry using an Accuri C6 (BD Biosciences). The data were analyzed using the FlowJo
500 software (Flow Jo LLC). When indicated, cells were transfected with siRNA 24 hours prior to transfection with
501 I-Sce1 expression plasmid. For SA-GFP and the CRISPR-LMNA HDR assay that were done in U2OS SA-GFP
502 HHV-6B IE1, cells were seeded at 10 000 cells per well in 24-well plates and induced with 1 µg/mL of
503 doxycycline 24 hours post transfection with either I-Sce1 for SA-GFP assay or plasmid expressing Cas9 and
504 *LMNA* sgRNA (pX330-LMNAgRNA1) and CR2.1-mRuby-2-LMNA-Donor for CRISPR-LMNA HDR assay(43).
505 At 48 hours post-transfection, cells were harvested and GFP-positive cells quantified by flow cytometry. mRuby-
506 positive cells were analyzed by microscopy using a TIRF Ti-LAPP microscope (Nikon).
507
508 **Statistical analysis**

509 Quantification was done on 3 biological replicates. Unless stated otherwise, one-way ANOVA with Dunnett's
510 multiple comparisons test were realized to assess statistical significance.
511

512 **Acknowledgement**

513 We are grateful to Matthew D. Weitzman, Alexandre Orthwein, Cary A. Moody and members of the A.F.-T. and
514 L.F. laboratory for critical reading of the manuscript; and to Daniel Durocher, Jean-Yves Masson, Graham
515 Dellaire, Roger Greenberg, and Jeremy Stark for essential reagents such as plasmids, purified proteins, and
516 cell lines. E.B, and V.C. received a postdoctoral and a doctoral fellowship from the Fonds de Recherche du
517 Québec - Santé (FRQS), respectively. V.T. received a master fellowship from the Fonds de recherche Nature
518 et technologies (FQRNT). This work was supported by three Canadian Institutes of Health Research Grants
519 (PDT_152948 to A.F.-T., and MOP_123214 and PJT_156118 to L.F.). A.F.-T. is a tier 2 Canada Research Chair
520 in Molecular Virology and Genomic Instability and is supported by the Foundation J.-Louis Lévesque. We thank
521 the Bioimaging platform of the Infectious Disease Research Centre, funded by an equipment and infrastructure
522 grants from the Canadian Foundation Innovation (CFI).
523

524 **Author Contributions:** V.C., E.B., L.F. and A.F.-T. designed research; V.C., E.B., V.T., E.G.L., J.D. and A.G.
525 performed research and analyzed data; V.C. and A.F.-T. wrote the original draft and E.B., and L.F. edited the
526 manuscript**.**
527

528 **Competing Interest Statement:** The authors declare no conflict of interest.
529

530 **References**

531 1. K. Yamanishi, *et al.*, Identification of Human Herpesvirus-6 As a Causal Agent for Exanthem Subitum.
532 *The Lancet* **331**, 1065–1067 (1988).

533 2. D. M. Zerr, *et al.*, A Population-Based Study of Primary Human Herpesvirus 6 Infection. *New England*
534 *Journal of Medicine* **352**, 768–776 (2005).

535 3. C. B. Hall, *et al.*, Congenital infections with human herpesvirus 6 (HHV6) and human herpesvirus 7
536 (HHV7). *Journal of Pediatrics* **145**, 472–477 (2004).

537 4. S. N. Pantry, P. G. Medveczky, Latency, integration, and reactivation of human herpesvirus-6. *Viruses*
538 **9** (2017).

539 5. J. H. Arbuckle, *et al.*, Mapping the telomere integrated genome of human herpesvirus 6A and 6B.
540 *Virology* **442**, 3–11 (2013).

541 6. J. H. Arbuckle, *et al.*, The latent human herpesvirus-6A genome specifically integrates in telomeres of
542 human chromosomes in vivo and in vitro. *Proceedings of the National Academy of Sciences of the*
543 *United States of America* **107**, 5563–5568 (2010).

544 7. K. Tanaka-Taya, *et al.*, Human herpesvirus 6 (HHV-6) is transmitted from parent to child in an
545 integrated form and characterization of cases with chromosomally integrated HHV-6 DNA. *Journal of*
546 *Medical VirologyThe prevalence of chromosomally integrated human herpesvirus 6 genomes in the*
547 *blood of UK blood donors.* **73**, 465–473 (2004).

548 8. M. Daibata, T. Taguchi, Y. Nemoto, H. Taguchi, I. Miyoshi, Inheritance of chromosomally integrated
549 human herpesvirus 6 DNA. *Blood* **94**, 1545–1549 (1999).

550 9. S. Minocherhomji, *et al.*, Replication stress activates DNA repair synthesis in mitosis. *Nature* **528**
551 (2015).

552 10. F. Gaccioli, *et al.*, Fetal inheritance of chromosomally integrated human herpesvirus 6 predisposes the
553 mother to pre-eclampsia. *Nature Microbiology* **5** (2020).

554 11. A. Gravel, *et al.*, Inherited chromosomally integrated human herpesvirus 6 as a predisposing risk
555 factor for the development of angina pectoris. *Proceedings of the National Academy of Sciences of*
556 *the United States of America* **112** (2015).

557 12. P. E. Pellett, Chromosomally integrated human herpesvirus 6: questions and answers. *Reviews in*
558 *medical virology* **22**, 144–55 (2012).

559 13. L. Flamand, "Chromosomal integration by human herpesviruses 6A and 6B" in *Advances in*
560 *Experimental Medicine and Biology*, (2018).

561 14. N. Wallaschek, *et al.*, The Telomeric Repeats of Human Herpesvirus 6A (HHV-6A) Are Required for
562 Efficient Virus Integration. *PLoS Pathogens* **12**, 1–15 (2016).

563 15. G. Aimola, G. Beythien, A. Aswad, B. B. Kaufer, Current understanding of human herpesvirus 6 (HHV-
564 6) chromosomal integration. *Antiviral Research* **176** (2020).

565 16. G. Morissette, L. Flamand, Herpesviruses and Chromosomal Integration. *Journal of Virology* **84** (2010).

566 17. V. Collin, L. Flamand, HHV-6A/B integration and the pathogenesis associated with the reactivation of
567 chromosomally integrated HHV-6A/B. *Viruses* **9** (2017).

568 18. A. Syed, J. A. Tainer, The MRE11-RAD50-NBS1 Complex Conducts the Orchestration of Damage
569 Signaling and Outcomes to Stress in DNA Replication and Repair. *Annual Review of Biochemistry* **87**
570 (2018).

571 19. A. Fradet-Turcotte, *et al.*, 53BP1 is a reader of the DNA-damage-induced H2A Lys 15 ubiquitin mark.
572 *Nature* **499** (2013).

573 20. F. Mattiroli, L. Penengo, Histone Ubiquitination: An Integrative Signaling Platform in Genome
574 Stability. *Trends in Genetics* (2021) https:/doi.org/10.1016/j.tig.2020.12.005.

575 21. A. Maréchal, L. Zou, DNA damage sensing by the ATM and ATR kinases. *Cold Spring Harbor*
576 *Perspectives in Biology* **5** (2013).

577 22. R. Bhargava, D. O. Onyango, J. M. Stark, Regulation of Single Strand Annealing and its role in genome
578 maintenance Chromosomal break repair by the Single Strand Annealing (SSA) pathway. *Trends Genet*
579 **32**, 566–575 (2016).

580 23. Z. W. Kockler, B. Osia, R. Lee, K. Musmaker, A. Malkova, Repair of DNA Breaks by Break-Induced
581 Replication. *Annual Review of Biochemistry* **90** (2021).

582 24. A. Gravel, *et al.*, Mapping the Human Herpesvirus 6B transcriptome. *Journal of Virology* (2021)
583 https:/doi.org/10.1128/JVI.01335-20.

584 25. U. Schiewe, F. Neipel, D. Schreiner, B. Fleckenstein, Structure and transcription of an immediate-early
585 region in the human herpesvirus 6 genome. *J Virol* **68**, 2978–2985 (1994).

586 26. J. Jaworska, A. Gravel, L. Flamand, Divergent susceptibilities of human herpesvirus 6 variants to type I
587 interferons. *Proceedings of the National Academy of Sciences of the United States of America* **107**,
588 8369–8374 (2010).

589 27. J. Jaworska, A. Gravel, K. Fink, N. Grandvaux, L. Flamand, Inhibition of Transcription of the Beta
590 Interferon Gene by the Human Herpesvirus 6 Immediate-Early 1 Protein. *Journal of Virology* **81**,
591 5737–5748 (2007).

592 28. R. Bernardi, P. P. Pandolfi, Structure, dynamics and functions of promyelocytic leukaemia nuclear
593 bodies. *Nature Reviews Molecular Cell Biology* **8**, 1006–1016 (2007).

594 29. P. L. Yeung, *et al.*, Promyelocytic leukemia nuclear bodies support a late step in DNA double-strand
595 break repair by homologous recombination. *Journal of Cellular Biochemistry* **113**, 1787–1799 (2012).

596 30. K. M. Attwood, *et al.*, PML isoform expression and DNA break location relative to PML nuclear bodies
597 impacts the efficiency of homologous recombination. *Biochemistry and Cell Biology*, 1–42 (2019).

598 31. G. Dellaire, *et al.*, Promyelocytic leukemia nuclear bodies behave as DNA damage sensors whose
599 response to DNA double-strand breaks is regulated by NBS1 and the kinases ATM, Chk2, and ATR.
600 *Journal of Cell Biology* **175**, 55–66 (2006).

601 32. M. Vancurova, *et al.*, PML nuclear bodies are recruited to persistent DNA damage lesions in an
602 RNF168-53BP1 dependent manner and contribute to DNA repair. *DNA Repair* **78** (2019).

603 33. V. Collin, A. Gravel, B. B. Kaufer, L. Flamand, The promyelocytic leukemia protein facilitates human
604 herpesvirus 6B chromosomal integration, immediate-early 1 protein multiSUMOylation and its
605 localization at telomeres. *PLoS Pathogens* **16** (2020).

606 34. S. Gilbert-Girard, *et al.*, Stabilization of telomere G-quadruplexes interferes with human herpesvirus
607 6A chromosomal integration. *Journal of Virology*, JVI.00402-17 (2017).

608 35. A. Gravel, *et al.*, Cell Culture Systems To Study Human Herpesvirus 6A/B Chromosomal Integration.
609 *Journal of Virology* **91**, e00437-17 (2017).

610 36. A. P. R. Cassel, R. B. Barcellos, C. M. D. da Silva, S. E. de Matos Almeida, M. L. R. Rossetti, Association
611 between human papillomavirus (HPV) DNA and micronuclei in normal cervical cytology. *Genetics and*
612 *Molecular Biology* **37**, 360–363 (2014).

613 37. V. Collin, A. Gravel, B. B. Kaufer, L. Flamand, The promyelocytic leukemia protein facilitates human
614 herpesvirus 6B chromosomal integration, immediate-early 1 protein multiSUMOylation and its
615 localization at telomeres. *PLoS Pathogens* **16** (2020).

616 38. J. Sitz, *et al.*, Human papillomavirus E7 oncoprotein targets RNF168 to hijack the host DNA damage
617 response. *Proceedings of the National Academy of Sciences of the United States of America* **116**
618 (2019).

619 39. J. Tang, *et al.*, Acetylation limits 53BP1 association with damaged chromatin to promote homologous
620 recombination. *Nature Structural and Molecular Biology* **20**, 317–325 (2013).

621 40. L. Bian, Y. Meng, M. Zhang, D. Li, MRE11-RAD50-NBS1 complex alterations and DNA damage
622 response: Implications for cancer treatment. *Molecular Cancer* **18** (2019).

623 41. E. Soutoglou, T. Misteli, Activation of the cellular DNA damage response in the absence of DNA
624 lesions. *Science* **320** (2008).

625 42. J. M. Stark, A. J. Pierce, J. Oh, A. Pastink, M. Jasin, Genetic Steps of Mammalian Homologous Repair
626 with Distinct Mutagenic Consequences. *Molecular and Cellular Biology* **24**, 9305–9316 (2004).

627 43. R. A. C. M. Boonen, *et al.*, Functional analysis of genetic variants in the high-risk breast cancer
628 susceptibility gene PALB2. *Nature Communications* **10** (2019).

629 44. L. Costantino, *et al.*, Break-induced replication repair of damaged forks induces genomic duplications
630 in human cells. *Science* **343**, 88–91 (2014).

631 45. M. D. Weitzman, A. Fradet-Turcotte, Virus DNA replication and the host DNA damage response.
632 *Annual Review of Virology* **5** (2018).

633 46. R. L. Dilley, *et al.*, Break-induced telomere synthesis underlies alternative telomere maintenance.
634 *Nature* **539** (2016).

635 47. V. Peddu, *et al.*, Inherited Chromosomally Integrated Human Herpesvirus 6 Demonstrates Tissue-
636 Specific RNA Expression In Vivo That Correlates with an Increased Antibody Immune Response .
637 *Journal of Virology* **94** (2019).

638 48. R. Xu, *et al.*, Mitosis-specific MRN complex promotes a mitotic signaling cascade to regulate spindle
639 dynamics and chromosome segregation. *Proceedings of the National Academy of Sciences of the*
640 *United States of America* **115** (2018).

641 49. T. H. Stracker, C. T. Carson, M. D. Weilzman, Adenovirus oncoproteins inactivate the Mre11-Rad50-
642 NBs1 DNA repair complex. *Nature* **418** (2002).

643 50. S. S. Mathew, E. Bridge, Nbs1-dependent binding of Mre11 to adenovirus E4 mutant viral DNA is
644 important for inhibiting DNA replication. *Virology* **374** (2008).

645 51. J. D. Evans, P. Hearing, Relocalization of the Mre11-Rad50-Nbs1 Complex by the Adenovirus E4 ORF3
646 Protein Is Required for Viral Replication. *Journal of Virology* **79** (2005).

647 52. K. A. Karen, P. J. Hoey, C. S. H. Young, P. Hearing, Temporal Regulation of the Mre11-Rad50-Nbs1
648 Complex during Adenovirus Infection. *Journal of Virology* **83** (2009).

649 53. S. S. Lakdawala, *et al.*, Differential Requirements of the C Terminus of Nbs1 in Suppressing Adenovirus
650 DNA Replication and Promoting Concatemer Formation. *Journal of Virology* **82** (2008).

651 54. R. A. Schwartz, *et al.*, The Mre11/Rad50/Nbs1 Complex Limits Adeno-Associated Virus Transduction
652 and Replication. *Journal of Virology* **81** (2007).

653 55. R. Millet, *et al.*, Impact of the MRN Complex on Adeno-Associated Virus Integration and Replication
654 during Coinfection with Herpes Simplex Virus 1. *Journal of Virology* **89** (2015).

655 56. D. C. Anacker, D. Gautam, K. A. Gillespie, W. H. Chappell, C. A. Moody, Productive Replication of
656 Human Papillomavirus 31 Requires DNA Repair Factor Nbs1. *Journal of Virology* **88**, 8528–8544
657 (2014).

658 57. D. E. Wilkinson, S. K. Weller, Recruitment of Cellular Recombination and Repair Proteins to Sites of
659 Herpes Simplex Virus Type 1 DNA Replication Is Dependent on the Composition of Viral Proteins
660 within Prereplicative Sites and Correlates with the Induction of the DNA Damage Response. *Journal of*
661 *Virology* **78** (2004).

662 58. K. N. Mohni, A. S. Mastrocola, P. Bai, S. K. Weller, C. D. Heinen, DNA Mismatch Repair Proteins Are
663 Required for Efficient Herpes Simplex Virus 1 Replication. *Journal of Virology* **85** (2011).

664 59. C. E. Lilley, C. T. Carson, A. R. Muotri, F. H. Gage, M. D. Weitzman, DNA repair proteins affect the
665 lifecycle of herpes simplex virus 1. *Proceedings of the National Academy of Sciences of the United*
666 *States of America* **102** (2005).

667 60. F. J. Hari, C. Spycher, S. Jungmichel, L. Pavic, M. Stucki, A divalent FHA/BRCT-binding mechanism
668 couples the MRE11-RAD50-NBS1 complex to damaged chromatin. *EMBO Reports* **11** (2010).

669 61. C. Lukas, *et al.*, Mdc1 couples DNA double-strand break recognition by Nbs1 with its H2AX-dependent
670 chromatin retention. *EMBO Journal* **23** (2004).

671 62. J. R. Chapman, S. P. Jackson, Phospho-dependent interactions between NBS1 and MDC1 mediate
672 chromatin retention of the MRN complex at sites of DNA damage. *EMBO Reports* **9** (2008).

673 63. K. Kim, T. W. Kirby, L. Perera, R. E. London, Phosphopeptide interactions of the Nbs1 N-terminal FHA-
674 BRCT1/2 domains. *Scientific Reports* **11** (2021).

675 64. C. Xu, *et al.*, Structure of a Second BRCT Domain Identified in the Nijmegen Breakage Syndrome
676 Protein Nbs1 and its Function in an MDC1-Dependent Localization of Nbs1 to DNA Damage Sites.
677 *Journal of Molecular Biology* **381** (2008).

678 65. D. I. Lou, *et al.*, An Intrinsically Disordered Region of the DNA Repair Protein Nbs1 Is a Species-Specific
679 Barrier to Herpes Simplex Virus 1 in Primates. *Cell Host and Microbe* **20** (2016).

680 66. M. Tigano, D. C. Vargas, S. Tremblay-Belzile, Y. Fu, A. Sfeir, Nuclear sensing of breaks in mitochondrial
681 DNA enhances immune surveillance. *Nature* **591** (2021).

682 67. R. A. Wu, H. E. Upton, J. M. Vogan, K. Collins, Telomerase mechanism of telomere synthesis. *Annual*
683 *Review of Biochemistry* **86** (2017).

684 68. A. J. Cesare, R. R. Reddel, Alternative lengthening of telomeres: Models, mechanisms and
685 implications. *Nature Reviews Genetics* **11** (2010).

686 69. Z. H. Zhong, *et al.*, Disruption of telomere maintenance by depletion of the MRE11/RAD50/NBS1
687 complex in cells that use alternative lengthening of telomeres. *Journal of Biological Chemistry* **282**
688 (2007).

689 70. W.-Q. Jiang, *et al.*, Suppression of Alternative Lengthening of Telomeres by Sp100-Mediated
690 Sequestration of the MRE11/RAD50/NBS1 Complex. *Molecular and Cellular Biology* **25** (2005).

691 71. G. Wu, X. Jiang, W. H. Lee, P. L. Chen, Assembly of functional ALT-associated promyelocytic leukemia
692 bodies requires nijmegen breakage syndrome 1. *Cancer Research* **63** (2003).

693 72. D. J. Wight, *et al.*, Viral proteins U41 and U70 of human herpesvirus 6A are dispensable for telomere
694 integration. *Viruses* **10** (2018).

695 73. N. Wallaschek, A. Gravel, L. Flamand, B. B. Kaufer, The putative U94 integrase is dispensable for
696 human herpesvirus 6 (HHV-6) chromosomal integration. *Journal of General Virology* **97** (2016).

697 74. G. Aimola, G. Beythien, A. Aswad, B. B. Kaufer, Current understanding of human herpesvirus 6 (HHV-
698 6) chromosomal integration. *Antiviral Research* **176** (2020).

699 75. S. Sakamoto, *et al.*, Homologous recombination repair is regulated by domains at the N- and C-
700 terminus of NBS1 and is dissociated with ATM functions. *Oncogene* **26** (2007).

701 76. R. Bhowmick, S. Minocherhomji, I. D. Hickson, RAD52 Facilitates Mitotic DNA Synthesis Following
702 Replication Stress. *Molecular Cell* **64** (2016).

703 77. Y. Huang, *et al.*, Human telomeres that carry an integrated copy of human herpesvirus 6 are often
704 short and unstable, facilitating release of the viral genome from the chromosome. *Nucleic Acids*
705 *Research* **42** (2014).

706 78. T.-H. Ho, *et al.*, A Screen for Epstein-Barr Virus Proteins That Inhibit the DNA Damage Response
707 Reveals a Novel Histone Binding Protein. *Journal of Virology* **92** (2018).

708 79. A. Orthwein, *et al.*, A mechanism for the suppression of homologous recombination in G1 cells.
709 *Nature* **528**, 422–426 (2015).

710 80. C. Escribano-Díaz, *et al.*, A Cell Cycle-Dependent Regulatory Circuit Composed of 53BP1-RIF1 and
711 BRCA1-CtIP Controls DNA Repair Pathway Choice. *Molecular Cell* **49**, 872–883 (2013).

712 81. D. C. Anacker, D. Gautam, K. A. Gillespie, W. H. Chappell, C. A. Moody, Productive Replication of
713 Human Papillomavirus 31 Requires DNA Repair Factor Nbs1. *Journal of Virology* **88**, 8528–8544
714 (2014).

715 82. F. P. Lopez C, Pellett P, Stewart J, Goldsmith C, Sanderlin K, Black J, Warfield D, Characteristics of
716 human herpesvirus-6. *The Journal of Infectious Diseases* **157**, 1271–1273 (1988).

717 83. A. Gravel, J. Gosselin, L. Flamand, Human herpesvirus 6 immediate-early 1 protein is a sumoylated
718 nuclear phosphoprotein colocalizing with promyelocytic leukemia protein-associated nuclear bodies.
719 *Journal of Biological Chemistry* **277**, 19679–19687 (2002).

720 84. J. M. Stark, A. J. Pierce, J. Oh, A. Pastink, M. Jasin, Genetic Steps of Mammalian Homologous Repair
721 with Distinct Mutagenic Consequences. *Molecular and Cellular Biology* **24**, 9305–9316 (2004).

722 85. R. Bhargava, *et al.*, C-NHEJ without indels is robust and requires synergistic function of distinct XLF
723 domains. *Nature Communications* **9** (2018).

724 86. K. Jacquet, *et al.*, The TIP60 Complex Regulates Bivalent Chromatin Recognition by 53BP1 through
725 Direct H4K20me Binding and H2AK15 Acetylation. *Molecular Cell* **62**, 409–421 (2016).

726 87. L. Costantino, *et al.*, Break-induced replication repair of damaged forks induces genomic duplications
727 in human cells. *Science* **343**, 88–91 (2014).

728 88. A. Gravel, *et al.*, Cell Culture Systems To Study Human Herpesvirus 6A/B Chromosomal Integration.
729 *Journal of Virology* **91**, e00437-17 (2017).

730

731 **Figure Legends**

732 **Fig. 1.** HHV-6B infection and IE1 expression leads to micronuclei formation. *(A)* Left panel: Representative
733 images of micronuclei observed in HHV-6B infected MOLT-3 cells. Cells were infected and fixed 24 hours post-

734 infection. DNA was counterstained with DAPI. Micronuclei are indicated by white arrows (scale bar, 5 µm).
735 Quantification of micronuclei are presented on the right panel. Data are presented as the mean (*n* = 2, >100
736 micronuclei/condition). *(B)* Left panel: representative images of U2OS cell line and U2OS clones stably
737 expressing doxycycline (Dox)-inducible HHV-6B IE1 protein (C10 and C102). Expression of IE1 was induced
738 for 48 hours with 1 µg/ml of Dox prior to fixation. Cells were then processed for IE1 immunofluorescence and
739 counterstained with DAPI. Micronuclei are indicated by white arrows (scale bar, 5 µm). Quantification of
740 micronuclei are presented on the right panel. The parental cell line (Par.) was used as a negative control and
741 data are presented as the mean ± SD (*n* = 3). *(C)* Schematic representation of the mechanisms leading to
742 micronuclei formation. Events leading to the formation of micronuclei induced by DNA double-strand breaks
743 (DSBs) (i) and lagging chromosome (ii) or by anaphase bridges (ABs) (iii) are represented. *(D-E)* Quantification
744 of micronuclei containing centromere (D) and telomere (E). Cells were treated as described in B and either
745 processed for centromere immunofluorescence or by FISH for the detection of telomeres. Data are presented
746 as mean ± SD (*n* = 3) (D) and as the mean (*n* = 2, >100 micronuclei/condition) (E). *(F)* Representative image of
747 a metaphase from IE1 expressing cells. Cells were exposed to 1 µg/ml of dox for 48 hours, metaphase spread
748 were prepared, fixed and processed for DNA counterstaining. *(G)* Quantification of chromosomal aberrations
749 per metaphase. Data were analyzed with an unpaired t-test and are presented as mean ± SD (*n* = 31). **p<0.01,
750 ***p<0.001, ****p<0.0001.
751
752 **Fig. 2.** Phosphorylation of H2AX (γ-H2AX) is inhibited in HHV-6B infected and IE1 expressing cells. *(A)*
753 Representative images of γ-H2AX in irradiated U2OS parental (Par.) and IE1-expressing cells. Cells were
754 treated as described in Fig. 1B and irradiated with 1 Gy. One hour post-irradiation, cells were fixed and
755 processed for IE1 and γ-H2AX immunofluorescence (scale bar, 5 µm). *(B)* Quantification of cells with more than
756 10 γ-H2AX foci in irradiated U2OS Par. and IE1expressing cells. Data are presented as the mean ± SD (*n* = 3).
757 *(C)* Quantification of cells with more than 10 γ-H2AX foci in U2OS $PML^{+/+}$ and $^{-/-}$ irradiated cells (1 Gy) that
758 transiently express untagged IE1. An empty vector (EV) was used as negative control. Data are presented as
759 the mean ± SD (*n* = 3). *(D)* Representative images of γ-H2AX in HHV-6B infected MOLT-3 cell lines. Cells were
760 irradiated with 4 Gy. One hour post-irradiation, cells were fixed and processed for IE1 and γ-H2AX
761 immunofluorescence (scale bar, 5 µm). Mock-infected cells were used as a negative control. *(E)* Quantification
762 of cells with more than 10 γ-H2AX foci in irradiated MOLT-3 infected cells. Data are presented as the mean ±
763 SD (*n* = 3) and statistical significance was assessed using unpaired t-test. ****p<0.0001.
764
765 **Fig. 3.** HHV-6B IE1 interacts with NBS1 and prevents its recruitment to DSBs. *(A, C)* Representative images of
766 the colocalization between NBS1 (A) and MRE11 (C) with IE1. IE1-expressing cells were treated as described
767 in Fig. 1B, fixed and processed for IE1, NBS1, or MRE11 immunofluorescence as indicated. As a positive
768 control, irradiated U2OS cells (+IR) were fixed 15 minutes post-irradiation (1 Gy) and processed for γ-H2AX,
769 NBS1, or MRE11 immunofluorescence as indicated (scale bar, 5 µm). The parental cell line (Par.) was used as
770 a negative control. *(B, D)* Quantification of γ-H2AX or IE1 foci that colocalized with NBS1 (B) and MRE11 (D)
771 are presented as percentage of foci per cells that colocalized with the indicated protein. Data are presented as
772 the mean ± SD of three independent experiments. *(E)* U2OS 2-6-5 cells transfected with plasmids expressing

773 the indicated mCherry-LacR fusion protein or induced for the expression of ER-mCherry-LacR-FokI-DD were
774 fixed and processed for NBS1 immunofluorescence (scale bars, 5 µm). The mCherry-LacR backbone was used
775 as a negative control (--). *(F)* Quantification of the mCherry-LacR foci colocalizing with NBS1 (E), γ-H2AX (*SI*
776 *Appendix,* Fig. S3*F*), and MRE11 (*SI Appendix,* Fig. S3G). Data are presented as the mean ± SD (*n* = 3).
777 ****p<0.0001.
778

779 **Fig. 4.** Bipartite binding and inhibition of NBS1 by HHV-6B IE1. *(A)* Schematic representation of HHV-6B IE1
780 protein and the fragments of the protein used in this study. NID, NBS1-interacting domain; NBS1i, NBS1
781 inhibitory domain, STAT2-BD: STAT2 binding-domain (aa 270-540). S432: CDK2 phosphorylation site. *(B)*
782 U2OS 2-6-5 cells transfected with the plasmids expressing the indicated mCherry-LacR fusion protein or
783 induced for the expression of ER-mCherry-LacR-FokI-DD were fixed and processed for NBS1
784 immunofluorescence (*SI Appendix,* Fig. S4A-B). The mCherry-LacR backbone was used as a negative control
785 (--). *(C)* Representative images of the inhibition of γ-H2AX by IE1. Cells were transiently transfected with the
786 indicated mCherry-LacR fusion protein and irradiated 24 hours later. One hour post-irradiation (1 Gy), cells were
787 fixed and processed for γ-H2AX immunofluorescence. The mCherry-LacR backbone was used as a negative
788 control (--) (scale bar, 5 µm). *(D)* Quantification of cells with more than 10 γ-H2AX foci. UT, untreated. Data for
789 *(B)* and *(D)* are presented as the mean ± SD (*n* = 3). *(E)* U2OS 2-6-5 cells were treated as described in (B),
790 processed for IE1 and γ-H2AX immunofluorescence (*SI Appendix,* Fig. S4E-F) and quantified as indicated. *(F)*
791 Schematic representation of NBS1 protein and the fragments of the protein used in this study. FHA, ForkHead-
792 Associated domain; BRCT, BRCA1 C-Terminal domain; MRE11-BM, MRE11-binding motif; ATM-BM, ATM-
793 binding motif; IDD, Intrinsically Disorder Domain. *(F-G)* U2OS 2-6-5 cells transfected with the plasmids
794 expressing the indicated mCherry-LacR and were fixed and processed. Data for *(E)* and *(G)* are presented as
795 the median ± SD (*n* = 3) (*E*). **p<0.01, ****p<0.0001.
796

797 **Fig. 5.** HHV-6B IE1 inhibits HDR-mediated repair. DNA repair reporter assays for *(A)* homologous
798 recombination (DR-GFP), *(B)* Single-strand annealing (SA-GFP), *(C)* Break-induced replication (BIR-GFP) and
799 *(D)* Non-homologous end-joining (NHEJ-GFP (EJ7)). For each condition, a schematic representation of the
800 assay is presented in the top panel and quantification of the GFP+ cells analyzed by flow cytometry is presented
801 in the bottom panel. GFP-positive cells are normalized over GFP-positive cells quantified in the positive control
802 (I-SceI+, set to 1.0) in each replicate. Data are represented as the mean ± SD (*n* = 3). ****p<0.0001.
803

804 **Fig. 6.** Depletion of NBS1 impairs viral integration in cells maintaining telomere by homology-directed repair.
805 *(A)* Schematic representation of HHV-6B infection in permissive and semi-permissive cells. In semi-permissive
806 cells for HHV-6B, where replication is inefficient, and the viral genome integrates at telomeres. *(B)* MOLT-3 cells
807 depleted or not for NBS1 were infected at a MOI of 1 with HHV-6B and harvested at the indicated time points.
808 Following cell lysis, DNA was extracted and the number of copies of HHV-6B were determined by qPCR using
809 primers for *U67-68* gene for HHV- 6B and *RPP30* as a cellular reference gene. Data presented are the mean
810 of three independent experiment and presented as mean ± SD (*n* = 3).
811

812 **Supplementary Figure Legends**

813 **Fig. S1.** *(A-B)* Whole cell extracts (WCE) from infected MOLT-3 (A) and U2OS cells treated or not with 1 µg/ml
814 of Dox (B) were analyzed by immunoblotting with an antibody against IE1. β-tubulin was used as loading control.
815 NI: non-infected, Par.: parental cell line. *(C, F, G)* Representative images of the U2OS (Par.) and U2OS IE1
816 stable cell lines with or without Dox induction (as indicated) for Figure 1B, D and E. Cells were treated as
817 described in Fig. 1B and either processed for IE1 (C, G) or centromeres (CREST) immunofluorescence (F) or
818 by FISH for the detection of telomeres (G) (scale bar, 5 µm). *(D-E)* U2OS (Par.) and U2OS IE1 stable cell lines
819 with Dox induction were treated as described in Fig. 1B and processed for Lamin B fluorescence. Quantification
820 of micronuclei with Lamin B signal is presented in (D) and representative images in (E). In (D), data are
821 represented as mean ± SD (*n* = 3) **p≤0.01. *(H)* Quantification of micronuclei colocalizing with IE1 foci. IE1-
822 expressing cells were treated as described in Fig. 1C, fixed and processed for IE1 immunofluorescence. Data
823 are presented as the mean ± SD (*n* = 2, >100 nuclei/condition).
824
825 **Fig. S2.** *(A)* Representative images of untreated U2OS $PML^{+/+}$ and $^{-/-}$ cells fixed and processed for PML
826 immunofluorescence. *(B)* Western blot analysis of U2OS transfected with untagged IE1 or an empty vector (EV)
827 plasmids WCE. β-tubulin was used as loading control. *(C)* Representative images of U2OS $PML^{+/+}$ and $^{-/-}$ cells
828 transiently transfected with a plasmid expressing untagged IE1 or an empty vector (EV) as negative control.
829 Cells were irradiated with 1 Gy, fixed 15 minutes post-irradiation and processed for IE1 and γ-H2AX
830 immunofluorescence (scale bar, 5 µm).
831
832 **Fig. S3**. *(A)* WCE from U2OS cells (Par.) and IE1-expressing U2OS stable cell lines treated or not with 1 µg/ml
833 of Dox were analyzed by immunoblotting with antibodies against RAD50, NBS1 and MRE11. GAPDH was used
834 as loading control. *(B-C)* Representative immunofluorescence of IE1-expressing U2OS stable cell lines induced
835 with Dox and irradiated with 1 Gy. Cells were fixed 1 hour post-irradiation and processed as described in Fig.
836 3A and C, respectively. *(D)* Quantification of IE1 foci that colocalize MRE11 in stable U2OS control cells
837 (shCTRL) or depleted for NBS1 (shNBS1). Cells were transiently transfected with untagged IE1 and treated as
838 described in Fig. 3B. Percentage of IE1 foci per cells that colocalize with NBS1 are presented as the mean ±
839 SD (*n* = 2, at least 40 nuclei/condition). **(E)** Representative immunofluorescence of the data presented in Fig.
840 Supp. 3D. *(F)* WCE from U2OS shCTRL and shNBS1 stable cell lines were analyzed by immunoblotting with
841 antibodies against NBS1 and MRE11. GAPDH was used as loading control. *(G-H)* Representative
842 immunofluorescence of the quantification presented in Fig. 3F. *(I)* Quantification of IE1 foci that colocalize with
843 NBS1 in U2OS $PML^{+/+}$ and $^{-/-}$ cells transiently expressing untagged IE1. Cells were treated as described in Fig.
844 3A. Percentage of IE1 foci per cells that colocalize with NBS1 are presented as the mean ± SD (*n* = 3). *(J)*
845 Representative immunofluorescence of the quantification presented in *SI Appendix,* Fig. S3I. Statistical
846 significance in (D) was assessed by unpaired t-tests, ****p<0.0001.
847
848 **Fig. S4.** *(A, D)* WCE from U2OS cells that transiently express the indicated mCherry-LacR fusion protein were
849 analyzed by immunoblotting with antibodies against mCherry. GAPDH was used as loading control. The
850 mCherry-LacR backbone was used as a negative control (--) in (A). *(B-C)* Representative immunofluorescence

851 images used for the quantification presented in Fig. 4B (B), Fig. 4D (C) (scale bar, 5 µm). *(E)* Representative
852 immunofluorescence images used for the quantification presented in Fig. 4E and Fig. Supp 4F (scale bar, 5
853 µm). *(F)* Quantification of mCherry-LacR foci dans colocalize with IE1. Data are presented as the median ± SD
854 (*n* = 3) ****p<0.0001. *(G)* Representative immunofluorescence images used for the quantification presented in
855 Fig. 4G and Fig. Supp 4H (scale bar, 5 µm)
856
857 **Fig. S5** *(A)* CRISPR-LMNA HDR assay was analyzed in Dox-inducible IE1 U2OS SA-GFP stable cell lines. Cell
858 lines were plated and induced for IE1 expression for 24 hours prior to transfection with plasmids encoding Cas9,
859 *LMNA* sgRNA, and mRuby2-LMNA donor. Percentage of mRuby-positive cells were analyzed by flow cytometry
860 48 h post-transfection and normalized over percentage of mRuby-positive U2OS SA cells (Par.) in each
861 replicate. *(B)* DNA repair assay for homologous recombination in HeLa cells were performed as described for
862 U2OS cells in Fig. 5A. *(C)* Single-strand annealing (SA) assay was analyzed in Dox-inducible IE1 U2OS SA-
863 GFP stable cell lines. Cell lines were plated and induced for IE1 expression for 24 hours prior to transfection
864 with plasmids encoding I-SceI endonuclease. Percentage of GFP-positive cells were analyzed by flow cytometry
865 48 h post-transfection and normalized over percentage of GFP-positive U2OS SA cells (Par.) in each replicate.
866 Data are represented as the mean ± SD (*n* = 2). *(D)* Validation of the BIR repair assay using siRNA against
867 RAD51 and RAD52. A non-targeting siRNA (NT) was also used as control. *(E-F)* RT-qPCR was performed on
868 U2OS BIR cells using gene-specific primers for *RAD51*(E) and *RAD52*(F). Expression of each transcript has
869 been normalized against *GADPH*. *(G)* DNA repair assay for non-homologous end-joining (NHEJ-pc222) in
870 U2OS cells were performed as described in Fig. 5D. Unless stated otherwise, data are represented as the mean
871 ± SD (at least n = 3). In (A), statistical significance was assessed by unpaired t-tests, **p<0.01, ***p<0.001,
872 ****p<0.0001.
873
874 **Fig. S6.** *(A-D)* WCE from MOLT-3 (A), HeLa (B), U2OS (C), and GM847 (D) cell lines expressing a shRNA
875 against NBS1 (shNBS1) or control (shCTRL) were analyzed by immunoblotting with an antibody against NBS1.
876 β-Tubulin was used as loading control.

Fig. 1

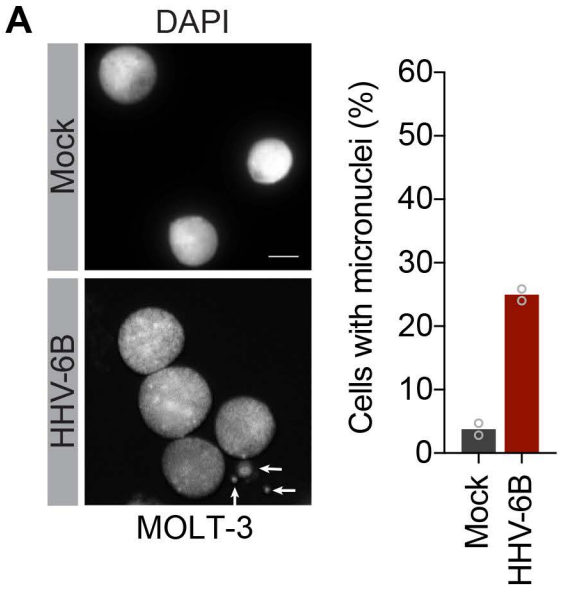
A
DAPI
Mock
HHV-6B
MOLT-3
Cells with micronuclei (%)
60
50
40
30
20
10
0
Mock
HHV-6B

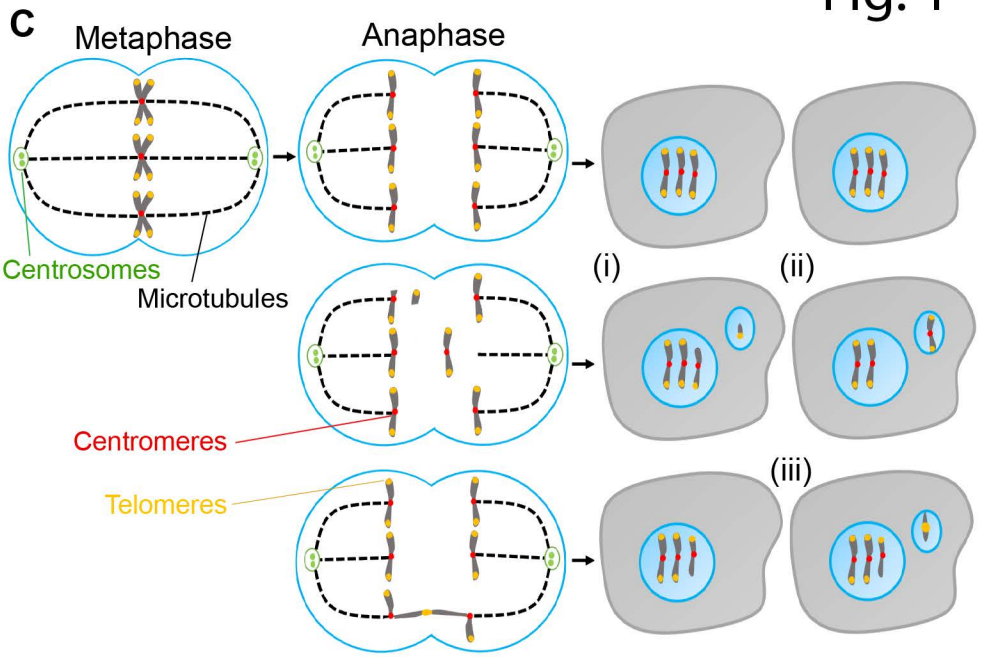
C
Metaphase
Anaphase
Centrosomes
Microtubules
Centromeres
Telomeres
(i)
(ii)
(iii)

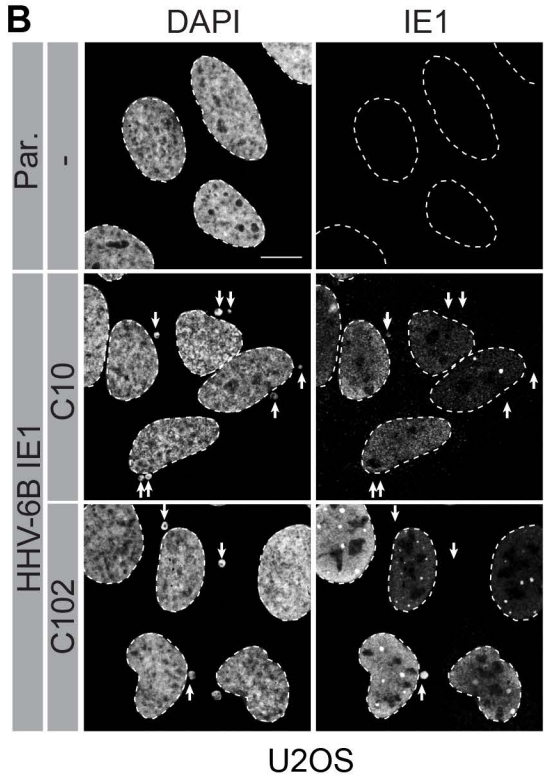
B
DAPI
IE1
Par.
-
HHV-6B IE1
C10
C102
U2OS

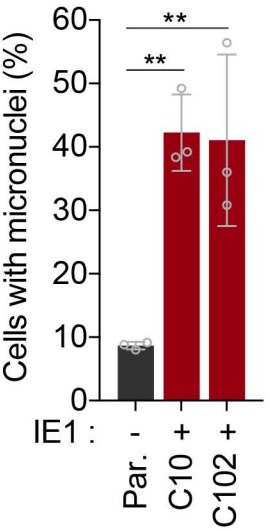
Cells with micronuclei (%)
60
50
40
30
20
10
0
**
**
IE1 :
-
+
+
Par.
C10
C102

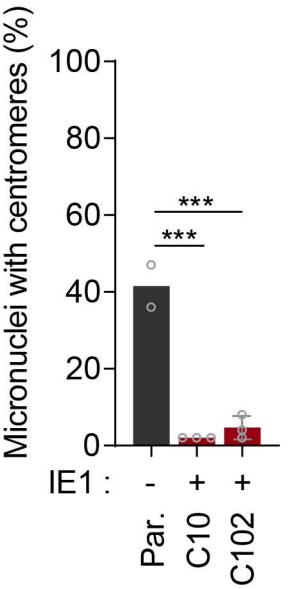
D
Micronuclei with centromeres (%)
100
80
60
40
20
0
***
***
IE1 :
-
+
+
Par.
C10
C102

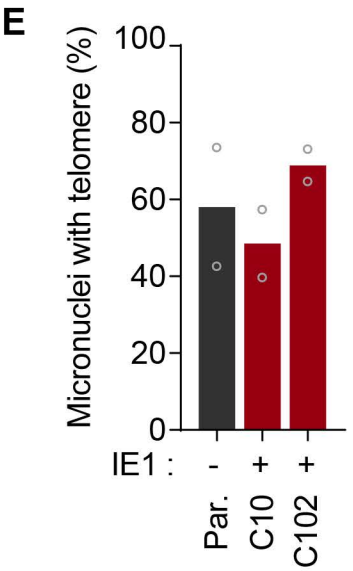
E
Micronuclei with telomere (%)
100
80
60
40
20
0
IE1 :
-
+
+
Par.
C10
C102

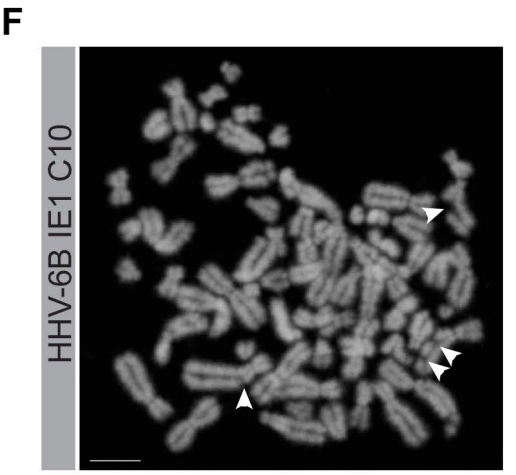
F
HHV-6B IE1 C10

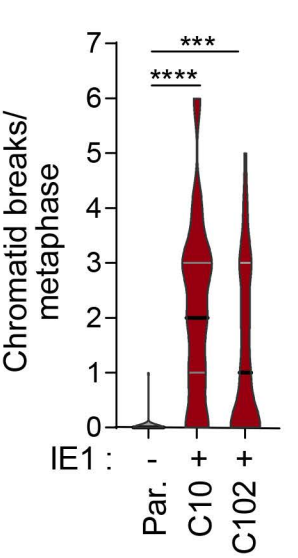
G
Chromatid breaks/
metaphase
7
6
5
4
3
2
1
0
***
****
IE1 :
-
+
+
Par.
C10
C102

Fig. 2

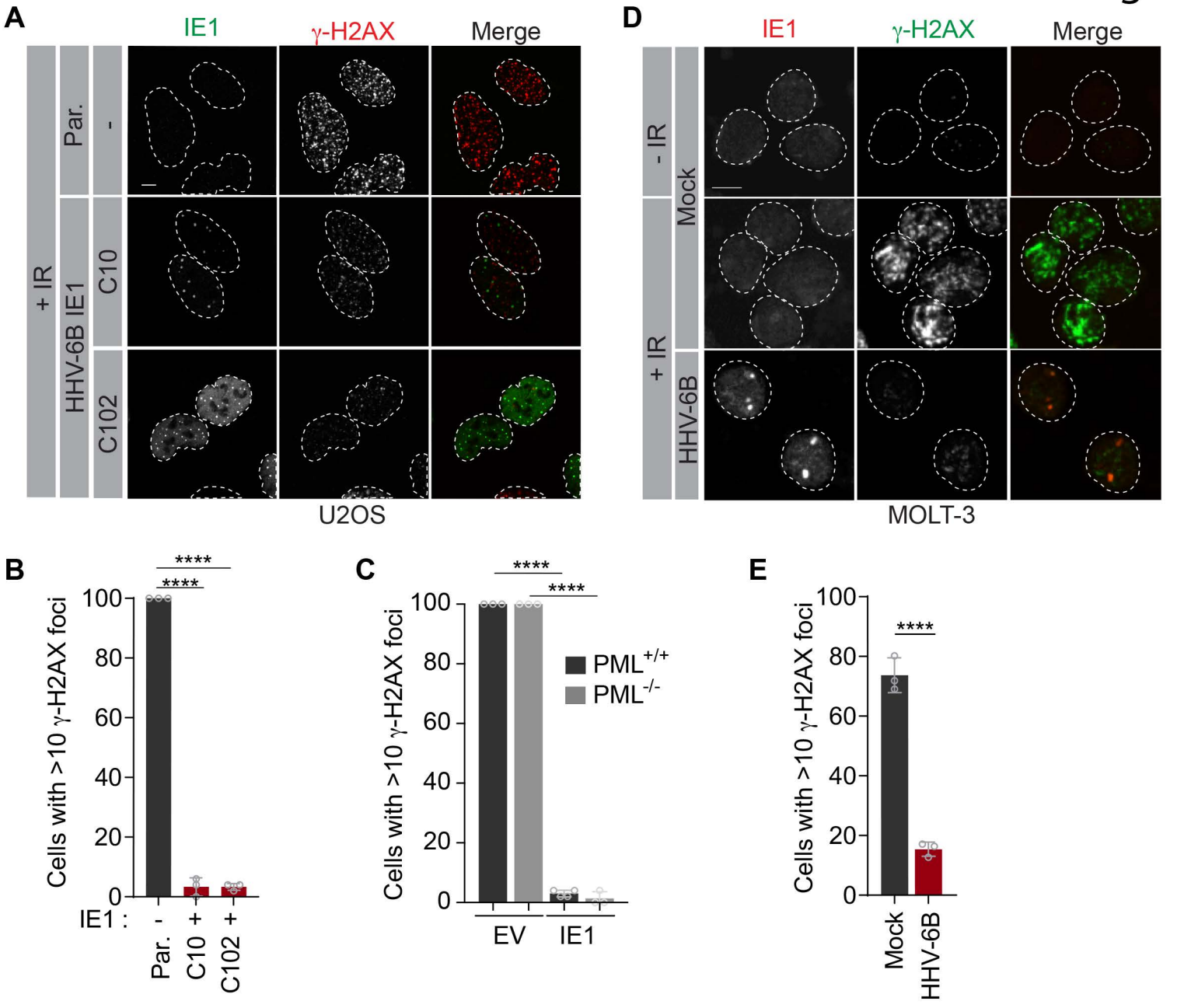
A
IE1
γ-H2AX
Merge
+ IR
Par.
-
HHV-6B IE1
C10
C102
U2OS
D
IE1
γ-H2AX
Merge
- IR
Mock
+ IR
HHV-6B
MOLT-3
B
Cells with >10 γ-H2AX foci
100
80
60
40
20
0
****
****
IE1 :
-
+
+
Par.
C10
C102
C
Cells with >10 γ-H2AX foci
100
80
60
40
20
0
****
****
PML+/+
PML-/-
EV
IE1
E
Cells with >10 γ-H2AX foci
100
80
60
40
20
0
****
Mock
HHV-6B

FIGURE 3

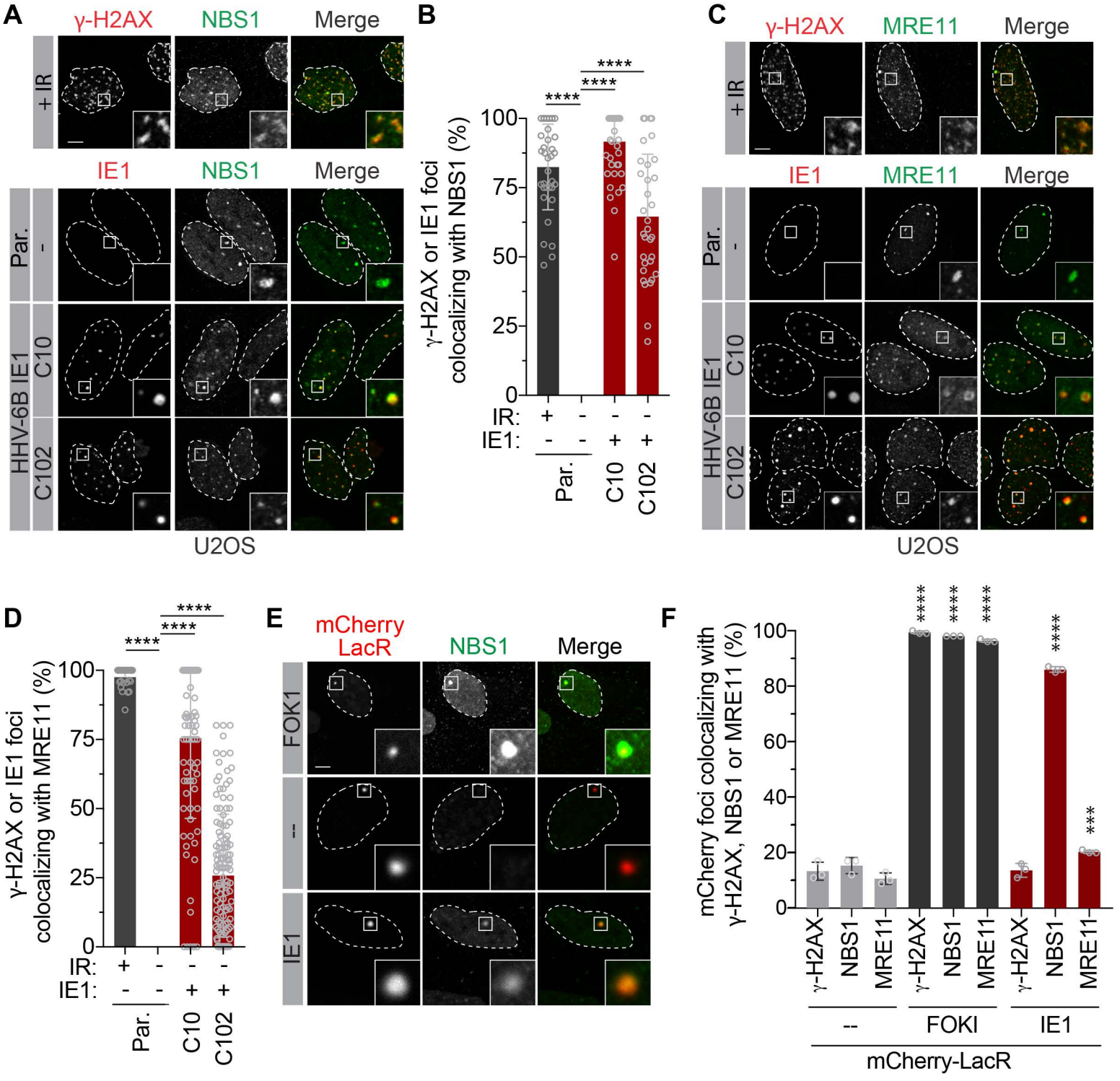
A
γ-H2AX
NBS1
Merge
+ IR
IE1
NBS1
Merge
Par.
-
HHV-6B IE1
C10
C102
U2OS
B
γ-H2AX or IE1 foci colocalizing with NBS1 (%)
100
75
50
25
0
****
****
****
IR: + - - -
IE1: - - + +
Par.
C10
C102
C
γ-H2AX
MRE11
Merge
+ IR
IE1
MRE11
Merge
Par.
-
HHV-6B IE1
C10
C102
U2OS
D
γ-H2AX or IE1 foci colocalizing with MRE11 (%)
100
75
50
25
0
****
****
****
IR: + - - -
IE1: - - + +
Par.
C10
C102
E
mCherry LacR
NBS1
Merge
FOK1
--
IE1
F
mCherry foci colocalizing with γ-H2AX, NBS1 or MRE11 (%)
100
80
60
40
20
0
****
****
****
****
***
γ-H2AX
NBS1
MRE11
γ-H2AX
NBS1
MRE11
γ-H2AX
NBS1
MRE11
--
FOKI
IE1
mCherry-LacR

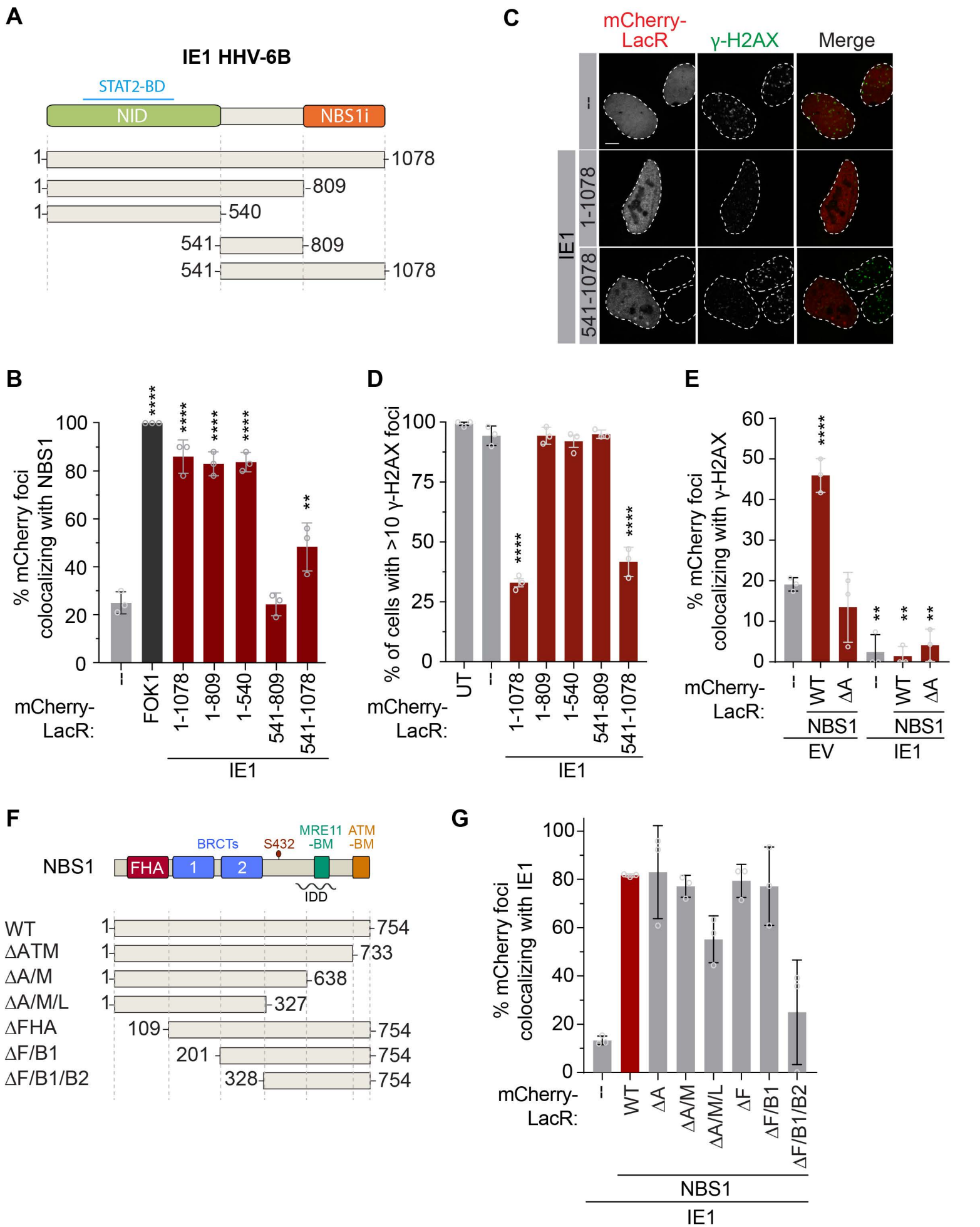
A
IE1 HHV-6B
STAT2-BD
NID
NBS1i
1-1078
1-809
1-540
541-809
541-1078
C
mCherry-LacR
γ-H2AX
Merge
IE1
--
1-1078
541-1078
B
% mCherry foci colocalizing with NBS1
mCherry-LacR:
--
FOK1
1-1078
1-809
1-540
541-809
541-1078
IE1
D
% of cells with >10 γ-H2AX foci
UT
E
% mCherry foci colocalizing with γ-H2AX
WT
ΔA
NBS1
EV
IE1
F
NBS1
FHA
BRCTs
S432
MRE11 -BM
ATM -BM
IDD
WT
ΔATM
ΔA/M
ΔA/M/L
ΔFHA
ΔF/B1
ΔF/B1/B2
G
% mCherry foci colocalizing with IE1
ΔF

Fig. 5

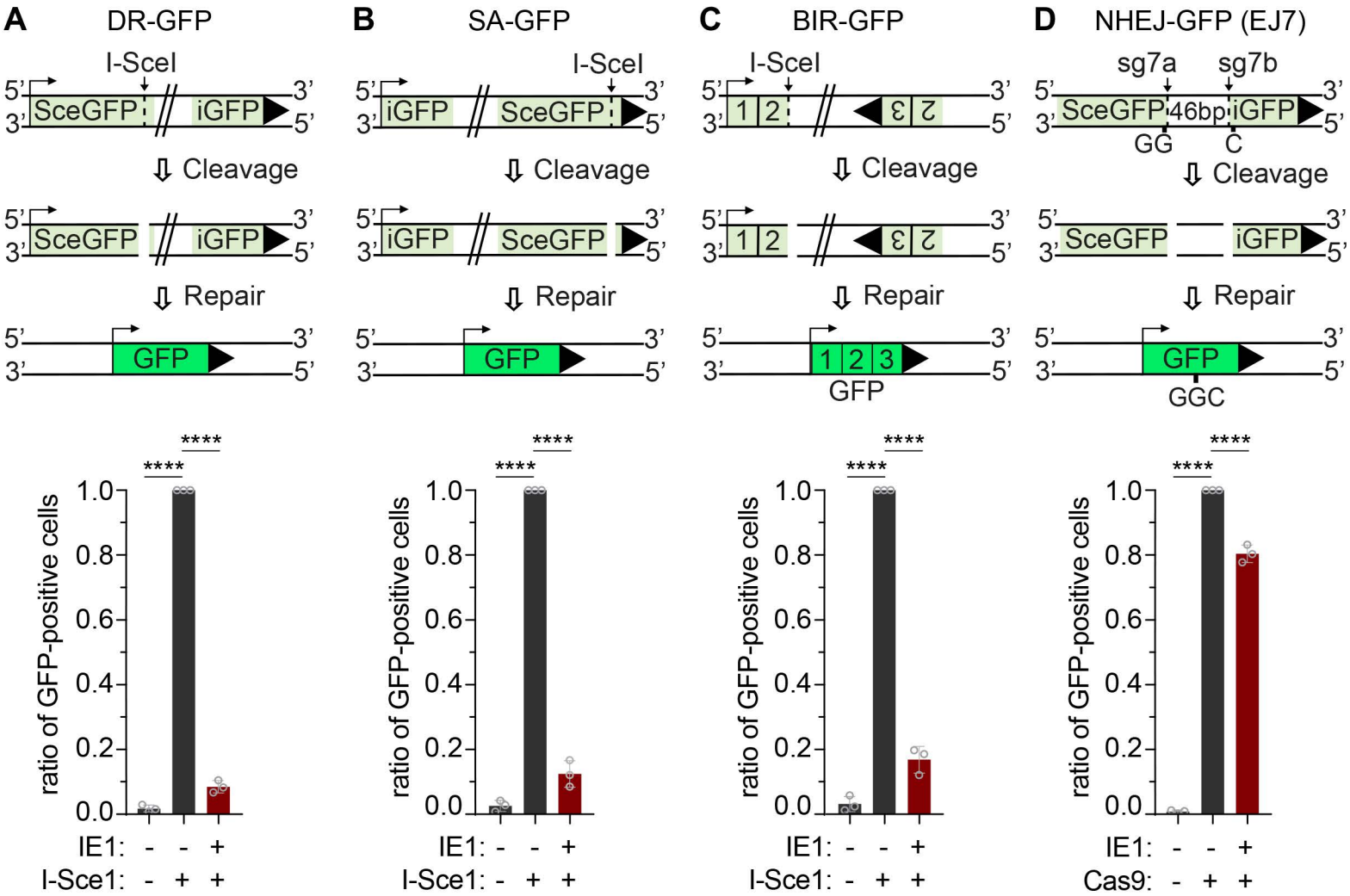
A
DR-GFP
I-SceI
SceGFP
iGFP
Cleavage
Repair
GFP
B
SA-GFP
I-SceI
iGFP
SceGFP
Cleavage
Repair
GFP
C
BIR-GFP
I-SceI
1
2
3
Cleavage
Repair
1
2
3
GFP
D
NHEJ-GFP (EJ7)
sg7a
sg7b
SceGFP
46bp
iGFP
GG
C
Cleavage
Repair
GFP
GGC
ratio of GFP-positive cells
****
IE1:
I-Sce1:
Cas9:

Fig. 6

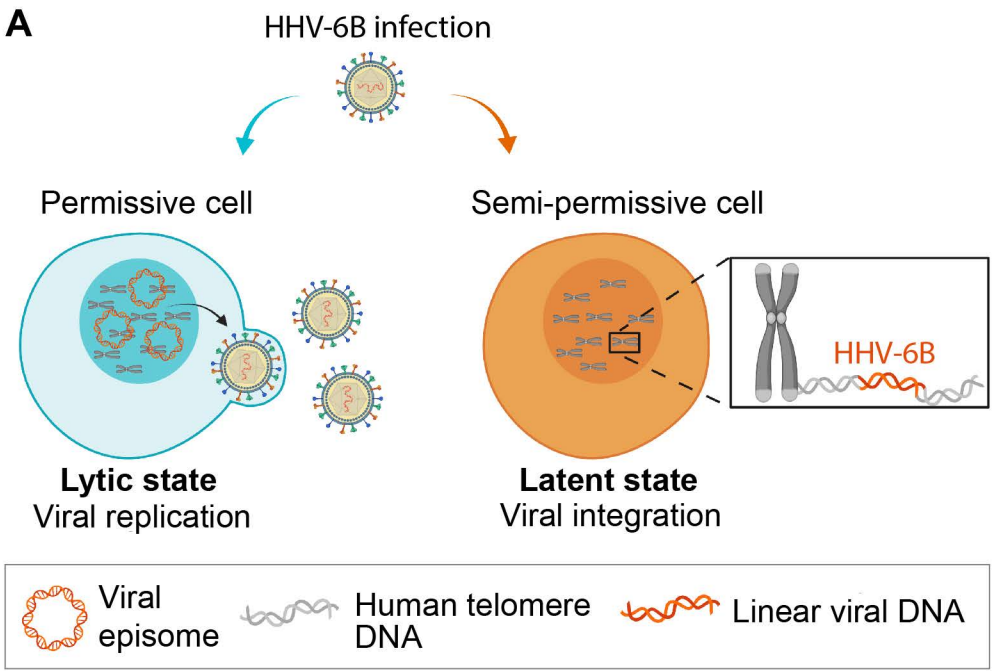
A
HHV-6B infection
Permissive cell
Semi-permissive cell
HHV-6B
Lytic state
Viral replication
Latent state
Viral integration
Viral episome
Human telomere DNA
Linear viral DNA

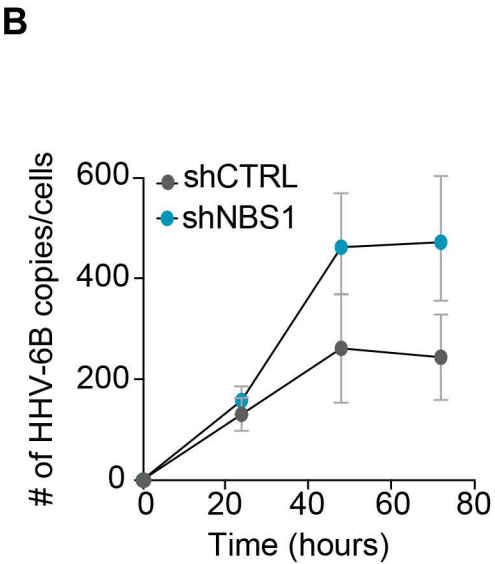
B
shCTRL
shNBS1
# of HHV-6B copies/cells
600
400
200
0
0
20
40
60
80
Time (hours)